A new interactive chemistry-climate model: 1. Present-day climatology and interannual variability of the middle atmosphere using the model and 9 years of HALOE/UARS data

B. Steil,[1] C. Brühl,[1] E. Manzini,[2,3] P. J. Crutzen,[1] J. Lelieveld,[1] P. J. Rasch,[4] E. Roeckner,[2] and K. Krüger[5]

Received 23 September 2002; revised 12 December 2002; accepted 24 January 2003; published 13 May 2003.

[1] The newly developed middle atmosphere general circulation model with interactive photochemistry, Middle Atmosphere European Centre/Hamburg Model 4 with Chemistry (MA-ECHAM4-CHEM), has been applied for several 20 year "time slice" experiments using fixed boundary conditions typical of the early and late 1990s, the 1960s, and the near future, including sensitivity runs to study effects of sea surface temperature and greenhouse gas concentration changes. In part 1 we compare the results for the early and late 1990s with 9 years of data of the Halogen Occultation Experiment (HALOE) on the Upper Atmosphere Research Satellite, some presented for the first time, and other satellite and radiosonde data. We show a statistical analysis as well as snapshots of a set of chemical species for typical situations. The model captures the main features of temperature and ozone distributions including the interannual variability of the Arctic and Antarctic vortices and homogeneous and heterogeneous ozone destruction. A detailed comparison of modeled and observed chlorine and nitrogen species including denitrification and chlorine repartitioning in the polar vortices is presented, showing generally good agreement. This holds also for chemical ozone budgets derived from the model and from satellite data. Computed stratospheric and mesospheric water vapor agrees with the satellite data within about 10%, including dehydration in the Antarctic winter. However, in the tropical lower stratosphere, the concentrations of the source gases are underestimated, presumably because of numerical deficiencies in transport. It is shown that interactive photochemistry is important to get agreement with observed temperatures in the lower stratosphere in high-latitude spring. Our coupled model provides a powerful tool to investigate chemical-radiative-dynamical feedback mechanisms of anthropogenic trace gas emissions and natural variability on climate and stratospheric ozone, at least for quasi-steady-state conditions. *INDEX TERMS:* 0340 Atmospheric Composition and Structure: Middle atmosphere—composition and chemistry; 0341 Atmospheric Composition and Structure: Middle atmosphere—constituent transport and chemistry (3334); 3337 Meteorology and Atmospheric Dynamics: Numerical modeling and data assimilation; 3319 Meteorology and Atmospheric Dynamics: General circulation; *KEYWORDS:* chemistry-climate model, stratospheric ozone, UARS satellite data, chlorine partitioning, polar ozone

Citation: Steil, B., C. Brühl, E. Manzini, P. J. Crutzen, J. Lelieveld, P. J. Rasch, E. Roeckner, and K. Krüger, A new interactive chemistry-climate model: 1. Present-day climatology and interannual variability of the middle atmosphere using the model and 9 years of HALOE/UARS data, *J. Geophys. Res.*, *108*(D9), 4290, doi:10.1029/2002JD002971, 2003.

1. Introduction

[2] Changes in greenhouse gas concentrations due to human activity modify the temperature distribution and dynamics of the middle atmosphere. The largest temperature changes have been observed near the stratopause and in the lower stratosphere in Antarctic spring [*Ramaswamy et al.*, 2001]. The chemistry of ozone is strongly temperature dependent. As a result of heterogeneous chlorine activation on Polar Stratospheric Clouds (PSC), cooling enhances catalytic ozone destruction in the polar lower stratosphere, while stratospheric gas phase chemistry is slowed down elsewhere, including catalytic ozone destruction. Ozone in turn controls net radiative heating of the middle atmosphere by absorption of solar UV and terrestrial IR radiation. Also water vapor in the stratosphere and mesosphere has a significant influence on the radiative cooling and on chem-

[1]Max Planck Institute for Chemistry, Mainz, Germany.
[2]Max Planck Institute for Meteorology, Hamburg, Germany.
[3]Now at National Institute for Geophysics and Volcanology, Bologna, Italy.
[4]National Center for Atmospheric Research, Boulder, Colorado, USA.
[5]Free University of Berlin, Berlin, Germany.

0148-0227/03/2002JD002971

istry. It is controlled mostly by physical processes at the tropical tropopause, the oxidation of methane, dehydration in Antarctic winter, transport and UV-radiation. Because of these complex interactions a fully interactive middle atmosphere (MA) chemistry-climate model is needed to study and predict atmospheric changes, including interactions between troposphere and stratosphere.

[3] Up to now most MA climate studies have been carried out with two-dimensional models or general circulation models (GCM) with highly parameterized chemistry [e.g., *Cariolle et al.*, 1990; *Shindell et al.*, 1998a, 1998b]. In addition, several short term integrations of GCMs with interactive chemistry have been performed [e.g., *Eckman et al.*, 1996; *Austin et al.*, 2000]. A transient simulation from near past to near future is presented by *Austin* [2002].

[4] *Shindell et al.* [1998a], using a model extending up to 80 km altitude, proposed that a cooling of the lower stratosphere and a circulation change in the upper troposphere due to increasing CO_2 might favor the formation of an Arctic ozone hole in the near future, despite the expected reduction in chlorine loading in response to the international regulations (Montreal Protocol). Their model, however, has a relatively coarse resolution and was run with strongly simplified chemistry.

[5] A first attempt by *Dameris et al.* [1998] to use a GCM with full stratospheric chemistry to simulate climate change scenarios focussed on the lower stratosphere since their model had its top at about 30 km. *Hein et al.* [2001] analyzed the interannual variability of the polar lower stratosphere in both hemispheres running their GCM for 20 years indicating that the model captures much of the observed features because large stratospheric disturbances are forced in the troposphere. However, both studies ignored ''downward control'' of stratospheric dynamics [*Holton et al.*, 1995; *Haynes et al.*, 1991; *Rind et al.*, 1999], given that the mass meridional circulation extends into the mesosphere, affecting the concentrations of chemical tracers and temperatures in the polar vortex via downward transport, which cannot be reproduced by 30 km top models. Other existing chemistry-climate models are discussed in the overview by *Austin et al.* [2002].

[6] In this study we present a simulation with the recently developed fully interactive middle atmosphere chemistry GCM Middle Atmosphere European Centre/Hamburg Model 4 with Chemistry (MA-ECHAM4-CHEM), simulating in total more than 4 decades with fixed boundary conditions representing the early and late 1990s. The results are compared with about 9 years of data of the Upper Atmosphere Research Satellite allowing a detailed analysis of interannual variability of temperatures and chemical species. We show statistical analysis of temperature, ozone and water vapor based on monthly mean values, but also, with focus on partitioning of chemical species, 3-D snapshots for typical situations in Arctic and Antarctic spring in model and observations. The study includes the chemical budget for ozone and some discussion on model uncertainties.

[7] The model has been used also with boundary conditions for the recent past and near future. Results, including a comparison with observed trends, will be presented elsewhere in parts 2 [*Manzini et al.*, 2003] and 3 (in preparation).

2. Models and Design of the Simulation

2.1. Brief Description of the MAECHAM4 Model

[8] The Middle Atmosphere version of the ''European Centre/Hamburg Model 4'' (MA-ECHAM4) is an atmospheric GCM that extends from the surface to 0.01 hPa (about 80 km). Except for tracer advection it is a spectral global model that includes state-of-the-art physical parameterizations for radiative transfer, cumulus convection, stratiform clouds (prognostic), gravity wave processes, as well as boundary layer and free atmosphere turbulent processes. Triangular truncation at wave number 30 (T30, Gaussian Grid of $3.75^\circ \times 3.75^\circ$ and 39 vertical levels (L39, from the surface to 80 km) have been used. The vertical resolution in the lower stratosphere is about 2 km. The MA-ECHAM4 model is an upward extended version of the ECHAM4 model which originally had its top in the lower stratosphere (at 10 hPa, or 30 km). The ECHAM4 model has been widely used in studies of climate [e.g., *Roeckner et al.*, 1999; *Bengtsson et al.*, 1999; *Bacher et al.*, 1998] and tropospheric ozone [e.g., *Roelofs et al.*, 1997]. A detailed description of the model is given by *Roeckner et al.* [1996]. Most of the physical parameterizations and the basic structure are common to both ECHAM4 and MA-ECHAM4. Differences between the two models include the vertical coordinates, the location of the model top and the parameterization of momentum flux deposition due to gravity waves. The MA-ECHAM4 model parameterizations and the model structure are summarized by *Manzini and McFarlane* [1998].

[9] In the MA-ECHAM4 model the gravity wave parameterization consists of two parts, separately representing momentum flux deposition due to orographic gravity waves and a broad band spectrum of non-orographic gravity waves. A modified version of the *McFarlane* [1987] parameterization is used to account for the orographic gravity wave drag. The Doppler spread formulation of *Hines* [1997a, 1997b] is used to parameterize the effects of the broad band gravity wave spectrum. Aspects of the sensitivity of the middle atmosphere circulation to the specification of the gravity wave source spectrum used in the Doppler spread parameterization are discussed by *Manzini and McFarlane* [1998] and *Manzini et al.* [1997]. In the current simulations the gravity wave spectrum is launched close to the surface (third model level from the surface), with a root-mean-square wind speed of 1 ms^{-1} and an effective horizontal wave number depending on latitude. The gravity wave source spectrum does not depend on season and hemisphere. This configuration is very similar to that used in EXP2 of *Manzini and McFarlane* [1998], but for a smaller rms gravity wave wind speed (e.g., weaker gravity wave forcing).

2.2. Tracer Advection

[10] Chemical species are advected using the SPITFIRE (Split Implementation of Transport Using Flux Integral Representation) transport scheme [*Rasch and Lawrence*, 1998; *Mahowald et al.*, 2002]. The transport scheme uses a control volume approach to update each tracer via a sequence of one-dimensional operations in each spatial direction. The fundamental prognostic variable is the mean tracer density within each cell. Similar to a semi-Lagrangian method, the one-dimensional update is stable for Lipshitz

numbers <1 and any Courant number. The method proceeds by fitting a polynomial to the integral of the tracer density. The integral of the tracer density field is monotonic, and a monotonic polynomial is fitted to this integral function. The tracer flux through a grid cell boundary is estimated from evaluation of the mass integral at the boundaries and at the respective departure points of the cell air masses. The interpolation required to calculate the mass integral is done using a fourth-order accurate cubic interpolant. Fluxes are limited using the "Universal" flux limiter discussed by *Leonard et al.* [1995]. The one-dimensional scheme is thus similar to the PPM (piecewise parabolic method) of *Colella and Woodward* [1984] although the form of the monotonicity constraint is different. The errors associated with operator splitting are compensated for by using the techniques suggested by *Lin and Rood* [1996] and *Leonard et al.* [1996]. The result is a conservative scheme that is monotonic in the tracer density after each one-dimensional update. A small additional error is introduced by the spatial splitting for flow with Courant numbers greater than one. At each time step tracer and air densities are updated. The mixing ratio is then derived from the ratio of tracer to air density.

2.3. Stratospheric Chemistry Module

[11] The chemistry module comprehensively describes stratospheric ozone photochemistry as well as tropospheric background NO_x-HO_x-CH_4-CO-O_3 chemistry [*Steil et al.*, 1998; *Steil*, 1999]. It adopts the very efficient "family" technique allowing for time steps as large as 45 min. The chemical integration requires only 6% of total CPU time (NEC SX4 and Cray C90). The following species and families are advected (50% of total CPU time):

$$N_2O,\ CH_4,\ H_2,\ CO,\ CH_3O_2H,\ H_2O_2,\ HCl,\ ClONO_2,$$

$$CFC11,\ CFC12,\ CH_3Cl,\ CH_3CCl_3,\ CCl_4,$$

$$HNO_3 + \text{type I PSC}(NAT : HNO_3 \cdot 3H_2O),$$

$$H_2O + \text{type II PSC (ice)},$$

$$ClO_x = Cl + ClO + ClHO + 2 \cdot Cl_2O_2 + 2 \cdot Cl_2,$$

$$NO_x = N + NO + NO_2 + NO_3 + HNO_4 + 2 \cdot N_2O_5,$$

$$O_x = O_3 + O(^3P) + O(^1D).$$

[12] Family members, radicals (like HO_x = H + OH + HO_2) and intermediates of the methane oxidation chain are calculated analytically or by implicit integration of the chemical differential equations. 110 photochemical reactions are considered, including pathways between H_2 and H_2O in the mesosphere. Photolysis rates are calculated online using the fast and accurate scheme of *Landgraf and Crutzen* [1998] to interactively account for varying clouds and overhead ozone. For zenith angles between 88 and 93 degrees an extrapolation based on the parameterization by *Röth* [1992] is applied.

[13] For long-lived source gases the mixing ratios at the surface are prescribed; for relatively shorter-lived species like NO_x emissions are prescribed and deposition processes are taken into account. Chlorine from CFC-113 and CFC-22 is considered by increasing the surface mixing ratio of CFC-12 since the stratospheric lifetime of these organic chlorine compounds is similar so that individual advection is not needed. At the top, a zero-flux condition is applied for all species except NO_x. To account for the NO-flux from the thermosphere into the mesosphere a latitude-dependent seasonal cycle of NO + NO_2 mixing ratios is prescribed at the top two levels of the model obtained from HALOE measurements over the years 1992–99 (see web page of UARS/HALOE at http://haloedata.larc.nasa.gov).

[14] Heterogeneous reactions on PSCs of type I (nitric acid trihydrate, NAT), type II (ice), and on sulfate aerosol are included [*Steil et al.*, 1998]. The results of the experimental study by *Hanson and Mauersberger* [1988] are applied to determine when PSCs are thermodynamically possible, based on the simulated temperature and the mixing ratios of HNO_3 and H_2O. We do not consider a nucleation barrier for NAT and ice, arguing that the model just calculates synoptic temperatures and cannot resolve small-scale temperature fluctuations, for example in lee waves, which might produce the supercooling in the real atmosphere needed for particle formation [*Waibel et al.*, 1999]. Comparison of box-trajectory calculations with satellite data, applying the scheme involving only solid PSCs [*Brühl et al.*, 1998a, 1998b], indicates that on large scales simulated ozone depletion during polar winter and spring is in good agreement with results obtained with more recent schemes that additionally describe liquid PSCs (ternary solutions) [*Carslaw et al.*, 1997; *Solomon*, 1999].

[15] In the model it is assumed that ice forms on large NAT particles. Although the theory has not been proven in the laboratory, it is likely that the formation of NAT occurs when the icepoint is reached [*Carslaw et al.*, 1997]. Therefore the sedimentation velocity of NAT and ice is assumed to be identical if ice is present, otherwise sedimentation is neglected. The Stokes velocity of ice particles is calculated every time-step according to the changing radius due to condensation or evaporation of water vapor. This scheme may underestimate denitrification in the Arctic but is well suitable for the Antarctic lower stratosphere where ice particles occur frequently.

[16] The type II PSC scheme is slightly modified compared to *Steil et al.* [1998]. The particle number density of ice is chosen to be n_{ice} = 0.03 cm^{-3} below 48 hPa, 0.05 cm^{-3} between 48 and 37 hPa, and 0.1 cm^{-3} above 37 hPa. These values are higher than those recommended by *Drdla and Turco* [1991], to correct for the cold bias in the modeled Antarctic vortex preventing a too strong dehydration.

[17] The "standard" cloud parameterization scheme of ECHAM4 is replaced in the extratropical stratosphere by the explicit calculation of the sedimentation of ice to prevent extreme dehydration of the Antarctic polar vortex. The stratospheric sulfuric acid aerosol surface areas are calculated on the basis of the lower limit case (background aerosol conditions) of *World Meteorological Organization* (*WMO*) [1992].

2.4. Simulation Design

[18] The experiments were performed in a fully interactive mode; that is, changes in ozone chemistry feed back on the dynamics and temperatures via radiative heating, and

Table 1. Sea Surface Temperatures and Lower Boundary Conditions of Long-Lived Gases for the Two Scenarios

	1990	2000
SST period	1981–1990	1989–1999
CH_4	1.69 ppmv	1.75 ppmv
N_2O	310 ppbv	320 ppbv
organic chlorine	3.4 ppbv	3.7 ppbv
CO_2	353 ppmv	372 ppmv

calculated temperatures and advection of species affect the speed of chemical reactions. To account for the large interannual variability of a fully coupled free running GCM, the simulations were performed for twenty years after a spinup of about ten years using fixed lower boundary conditions for CO_2 and the chemically active source gases from *WMO* [1999] listed in Table 1. The two scenarios for chemical boundary conditions were selected to cover the range of the satellite observations which is important because of the nonlinearity of ozone destruction with respect to chlorine. The sea surface temperatures (SSTs) are specified following the GISS/HADLEY monthly mean climatologies based on averages over the preceding decades [*Rayner et al.*, 1996]. More details on the model sensitivity to SSTs will be presented in part 3 of this study (C. Brühl et al., manuscript in preparation, 2003). Model years referred to in the next sections refer to the integration time after spinup.

3. Satellite Observations

[19] In the following sections we mostly use profiles of chemical species and temperatures observed by the still operational Halogen Occultation Experiment (HALOE; *Russell et al.* [1993]), the Microwave Limb Sounder (MLS; *Barath et al.* [1993]) and the Cryogenic Limb Array Etalon Spectrometer (CLAES; *Roche et al.* [1993]) onboard of the Upper Atmosphere Research Satellite (UARS) which was launched in September 1991. We have selected 9 years of HALOE data from October 1992 to November 2000 for analysis of interannual variability, focussing on high-latitude spring. HALOE observes ozone and species involved, directly or as precursors, in its catalytic destruction ($NO + NO_2$, H_2O, CH_4, HCl and HF) simultaneously. It also provides the most recent long-term measurements of upper stratospheric and mesospheric temperatures [*Hervig et al.*, 1996] which is important since there is a trend due to increasing infrared cooling from CO_2 and less solar heating related to ozone destruction by the chlorofluorocarbons below the stratopause. For a detailed description of the HALOE data and coverage, see the UARS special issue of *Journal of Geophysical Research*, *101*(D6), 9539–10,473, 1996 [e.g., *Brühl et al.*, 1996]. For HALOE, it takes about a month to scan the entire globe; at high latitudes no observations are possible in winter and summer. In spring and fall there are periods where a hemisphere is scanned in less then two weeks, the belt poleward of about 45 degrees is covered in several days so that it is possible to produce maps of chemical species at various levels in the middle atmosphere. One has to be aware, however, that the structures on these maps can be distorted by atmospheric dynamics during the scan time. A further complication is that the time for the satellite to scan a specific latitude shifts by about 3 days from year to year due to the satellite's orbit. This and the low coverage prohibit analysis of statistically significant three-dimensional distributions. Nevertheless, the UARS-data are the best available for validation of middle atmosphere GCMs with chemistry with respect to interannual variability and tracer correlation patterns.

[20] Additionally, observations of the Total Ozone Mapping Spectrometer (TOMS) on different satellites, the CRISTA instrument on the Space Shuttle [*Riese et al.*, 1999], and very recently available information from the ILAS and POAM instruments are used.

4. Summer Chemistry in the Middle and Lower Stratosphere: Budgets

[21] Stratospheric ozone production and loss during summer is dominated by gas phase chemistry. In summer there is no transport barrier between the polar regions and midlatitudes and because of almost no planetary wave breaking the interannual variability of dynamics is small. These conditions are most suitable for validation of the scheme for homogeneous chemistry used in the GCM. In high latitudes and midlatitudes, ozone decreases from spring to fall because of catalysis by NO_x under polar daylight conditions in the altitude region between about 10 to 100 hPa [*Brühl and Crutzen*, 2000; *Crutzen and Brühl*, 2001]. Net chemical ozone production as well as the contributions to ozone destruction by the different catalytical cycles, as calculated by the model for June, are depicted in Figure 1 and agree well with the corresponding figures in the above papers obtained with a 2-D-model constrained by HALOE observations. This also holds for the other summer months not shown here. Differences in the middle stratosphere, concerning the net chemical production, are due to the fact that it consists of individual production and destruction terms which are 1 to 2 orders of magnitude larger. This implies that in the free running model ozone above about 15 hPa is close to photochemical steady state, which is often not exactly the case if ozone, nitrogen oxides and precursors of radicals are taken from observations because of experimental uncertainties [e.g., *Grooß et al.*, 1999]. The altitude of the zero line and the region with maximum ozone production is about the same for ECHAM and in the analysis by *Crutzen and Brühl* [2001]. In the lower stratosphere the region with net ozone destruction extends slightly to lower latitudes compared to *Crutzen and Brühl* [2001]. The individual loss terms due to NO_x, HO_x and O_x above about 30 hPa are slightly smaller in ECHAM than in the "nudged" two-dimensional model.

[22] In the HALOE data as well as in the model results an anticorrelation between NO_x and ozone is apparent as shown for summer-day snapshots at the 30 hPa level in Figure 2 by scatter plots for sunset and sunrise (for orthographic maps of a similar situation see *Brühl et al.* [1998c]). Note that during sunrise in low latitudes a large fraction of NO_x is contained in the night-time reservoir species N_2O_5. As discussed later in more detail, because of transport deficiencies, NO_x in the model is slightly too low, and ozone is slightly too high (about 10%). The slopes, the latitude dependence, and other features of the correlation are approximately reproduced. For the sunrise example the differences in the slopes are larger than for sunset because

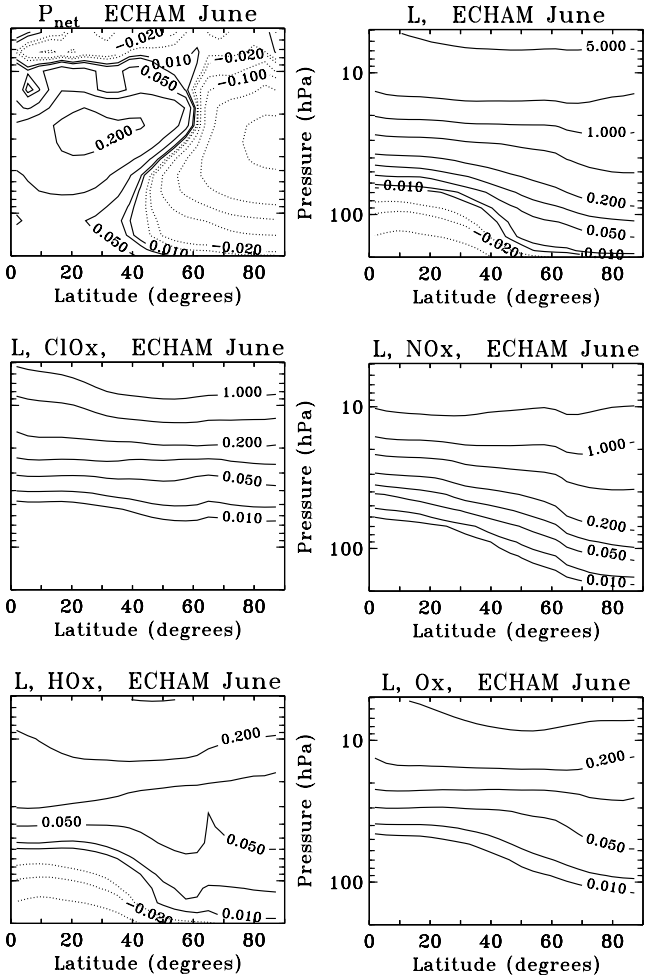

Figure 1. Net chemical ozone production (P_{net} = P-L with P chemical production from photolysis of molecular oxygen), chemical loss (L) and loss due to the different catalytical cycles (odd nitrogen, odd chlorine and odd hydrogen) in northern hemispheric summer (June average, in 10^6molecules/cm^3/s). As given by *Crutzen and Brühl* [2001], total loss (upper right panel) and the loss due to odd hydrogen (L, HOx) is corrected for the "photochemical smog" reactions which leads to negative values, i.e., a production, near the tropopause [*Crutzen and Schmailzl*, 1983]. L, Ox contains the Chapman reaction and reactions involving O(^{1}D).

the selected HALOE data set of 1994 was still effected by the Pinatubo eruption. Importantly, high-latitude summer chemistry in the altitude region between 30 and 10 hPa provides the initial conditions for the lower stratospheric processes in the vortex of the following winter.

5. Zonal Mean Structure

5.1. Total Ozone and Mean Temperatures

[23] The seasonal decline of total ozone from spring to fall in high northern latitudes is captured by the model as can be seen in Figure 3, which compares the 20 year average model results for total ozone (1990 time slice) with satellite observations by TOMS and HALOE. The model captures the main features like the maxima in midlatitude spring and the minima in the tropics. The decrease rate of ozone in Antarctic spring is as observed by TOMS (see also web site http://toms.gsfc.nasa.gov) but the absolute minima in the ozone hole are reached with a time lag of 10 days because of a high bias in midwinter in model total ozone. For most regions and seasons, calculated total ozone is high-biased with the largest differences up to about 20% in midlatitudes because of an overestimate of stratosphere to troposphere transport related to numerical deficiencies encountered in most of the existing spectral GCMs and Eulerian CTMs, see, for example, *Bregman et al.* [2002], *von Kuhlmann et al.* [2003], *Bey et al.* [2001], and section 8. By focusing on stratospheric ozone above 90 hPa alone, the differences are much smaller; however, there is still a high bias due to the underestimate of NO_x mentioned in the next sections, which is related to an underestimate of upward transport of N_2O, its main source gas, and due to underestimated upward transport of ozone poor tropospheric air in the tropics. The interannual variability of calculated total ozone compares well with that observed by TOMS. Similar conclusions hold for the 2000 time slice not shown here. In paper 2 [*Manzini et al.*, 2003] it is shown that also the observed seasonal and latitudinal distribution of total ozone trends are captured by the model.

[24] Monthly mean temperatures and their standard deviations (rms) at 50 hPa as function of season and latitude are very close to observations of the Free University of Berlin [*Pawson et al.*, 1993] as demonstrated in Figure 4 for the Northern Hemisphere and the early nineties. The model's rms is somewhat smaller in the tropics because of the missing Quasi Biannual Oscillation (QBO). It is slightly higher in the Arctic. The calculated cooling in March and slight warming in May in high latitudes for the 2000 time slice with respect to the previous decade is also present in the observations, as shown in Figure 4.

5.2. Vertical Distributions of Temperature and Gases

[25] We have compared calculated monthly average zonal mean vertical distributions of temperatures, ozone, water vapor, hydrogen chloride and the source gas methane with HALOE satellite data for the four seasons. For temperature, also the UKMO analysis was used, leading to similar differences as the comparison with the HALOE-data (which are in fact NCEP-analyses below about 10 hPa). HALOE temperature data might be more suitable for validation of the mesosphere and upper stratosphere than the CIRA climatology based on data of the seventies because of the trend due to growing greenhouse gases. Here we focus on the spring seasons in both hemispheres since these are the most relevant concerning feedbacks between chemistry and dynamics. Figure 5 shows October as representative example. Similar comparisons have been performed for January, April and July (not shown).

[26] Calculated average temperature distributions are very close to observations both in structure and absolute values for most regions. They show the maxima at the stratopause, and the minima near the tropical tropopause and in the Antarctic vortex in October, typically within about ±3 K. The largest differences up to about 10 K occur in the mesosphere in midlatitudes near the jet and in the Antarctic vortex in October between about 40 and 5 hPa, a region

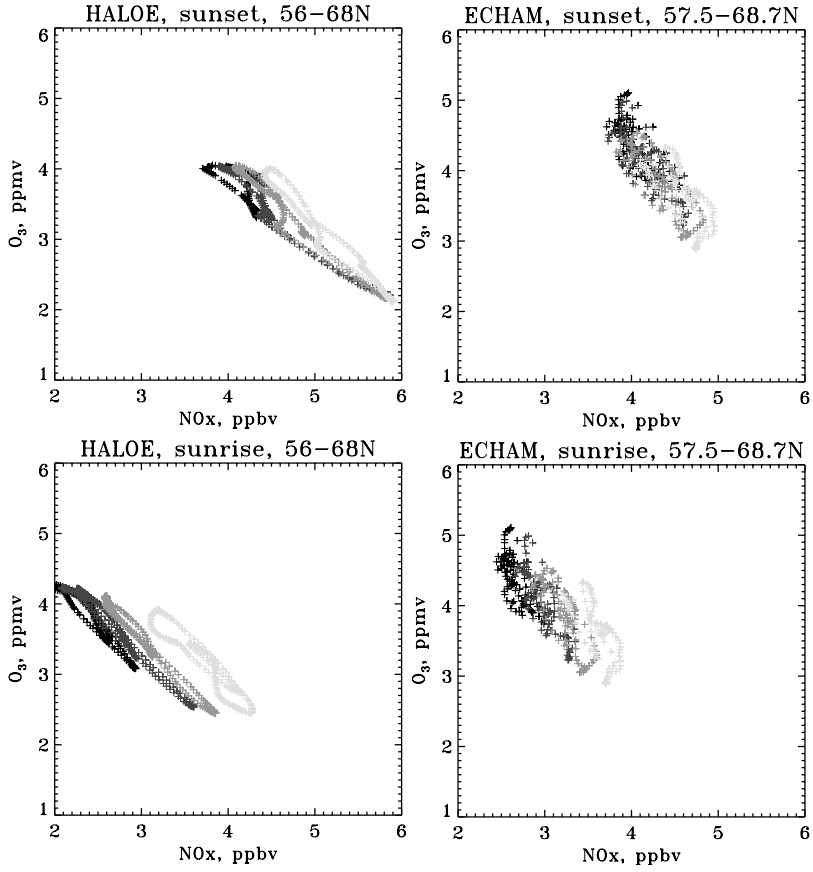

Figure 2. Anticorrelation between NO_x and O_3 at 30 hPa in high-latitude summer, mid August, as observed by HALOE (left) and calculated by MA-ECHAM in model year 4 of the 1990 scenario (right). Upper panels are for sunset (data from 1999), lower panels for sunrise (data from 1994). The grey-shades refer to latitude bins in steps of 4 degrees from 56 N (black) to 68 N (light grey). The average slopes for sunset are −1.1 ppm/ppb (HALOE) and −1.3 ppm/ppb (model), and for sunrise −1.3 ppm/ppb (HALOE) and −1.8 ppm/ppb (model).

where the vertical temperature gradients and the interannual variability are large. A detailed discussion of the polar temperature bias in chemistry-climate models has been presented by *Austin et al.* [2002]. Their Figure 3 shows that during December–January–February and March–April–May the MAECHAM4-CHEM model virtually has no cold bias at 80 N in the stratosphere, with respect to UKMO assimilated temperatures. At 80 S instead, depicted in the same figure, in the upper stratosphere the model develops a cold bias (of up to about 10 K), largest during September–October–November. As seen from the Austin intercomparison, the cold bias is present also in other models [see also *Pawson et al.*, 2000] and is due to insufficient gravity wave forcing.

[27] Calculated ozone is within ±15% compared to HALOE between about 30 and 0.1 hPa. In the mesosphere larger differences can be expected because of large variability and large diurnal cycles in chemistry, that are not well represented with our approach because of relative long lifetimes of O or OH radicals at sunset under upper mesospheric conditions. This leads to an overestimate of odd oxygen in the uppermost layer. This is, however, in the "damping layer" of the model and outside the aim of the study.

[28] The low-latitude ozone maximum at 10 hPa is slightly diluted toward midlatitudes, whereas the vertical gradient in the lowermost stratosphere is slightly too weak causing a relatively large percentage overestimate of ozone near the tropopause. Nevertheless the general patterns of ozone are well simulated including the Antarctic ozone hole.

[29] The comparison for water vapor (Figure 5, right) shows that the increase with height, caused by methane oxidation, as well as dehydration in the Antarctic vortex (October) and at the tropical tropopause are well captured. As observed, almost no dehydration in the Arctic vortex (April, not shown) is computed. The model also simulates the seasonal differences near the tropical tropopause. In polar spring the tropopause is too high and the vertical water vapor gradient is too weak. In the mesosphere the model captures the H_2O photolysis by Ly-radiation but not the secondary maximum at 70 km in the HALOE data. We emphasize, however, that the latter feature is quite uncertain and controversial [e.g., *Summers et al.*, 1997].

[30] The underestimated upward transport in the lower stratosphere of the tropics, which is also common in other models [e.g., *Rotman et al.*, 2001; *Hall et al.*, 1999; *Douglass et al.*, 1999], is best discernable using methane

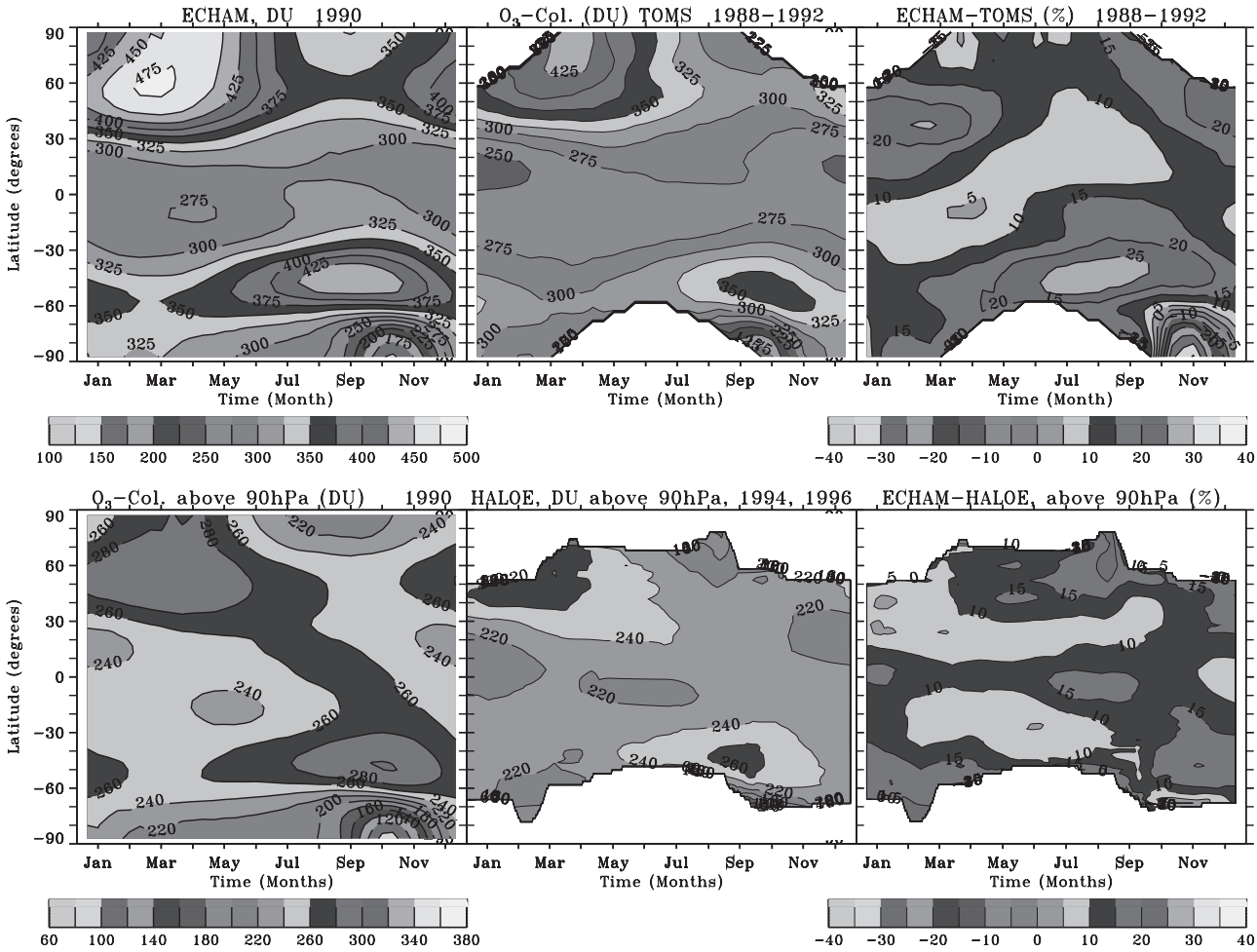

Figure 3. Total ozone in Dobson Units. Upper panels: Total ozone above surface, middle: 5 yr average of TOMS-observations, left: 20 yr average of ECHAM simulations (early 1990s), right: percentage differences. Lower panels: Total stratospheric ozone above 90 hPa, middle: 2 years of HALOE data (average of warm and cold Arctic winter), left: 20 yr average of ECHAM simulations, right: percentage differences. White areas indicate no data.

as tracer, as shown in Figure 6. In the model too little methane reaches the middle and upper stratosphere. The relatively steep gradients at the edge of the polar vortex and at the subtropical barrier are approximately as observed, although the absolute numbers have a negative bias. The underestimate of methane also causes a slight "low bias" in upper stratospheric water vapor. The same problem affects simulations of N_2O which is the dominant source of reactive nitrogen in the stratosphere. Calculated NO + NO_2 mixing ratios (dominating species of NO_x) in Figure 6 are therefore too low by about 10% although the overall pattern is well represented. The biases in the decay products are much smaller than for the source gases since most of the conversion occurs in the lower tropical stratosphere. The low bias in stratospheric reactive nitrogen is also seen in HNO_3 as discussed in the section on the polar regions. The large overestimate of NO_x above the tropical tropopause is consistent with too weak upward motion. Figure 6 also presents the comparison for HCl, indicating that the model simulates the heterogeneous conversion to reactive chlorine in the Antarctic ozone hole region approximately correct. The total amount of chlorine in the upper stratosphere derived from CFCs and CH_3Cl is consistent with observations. This is also the case for the downward transport of inorganic chlorine species in high-latitude winter and spring. The large percentage differences above the tropical tropopause, associated with transport deficiencies, have very little consequences because of the very low absolute concentrations of HCl and other inorganic chlorine species there.

5.3. Stratospheric Dynamics and Effects of Interactive Chemistry

[31] To diagnose horizontal transport barriers in a climatological sense, the model results for 20 years of CH_4 and N_2O are analyzed as done by *Sparling* [2000] using probability density functions of mixing-ratio-bins for different levels in the stratosphere (between 10 and 30 hPa) and different months. The patterns we get are very similar as in their analysis as shown in Figure 7. In this representative example for N_2O at 14 hPa in August, we get the peaks for vortex air, surfzone and tropics in the winter hemisphere, and tropics and extratropics in the summer hemisphere,

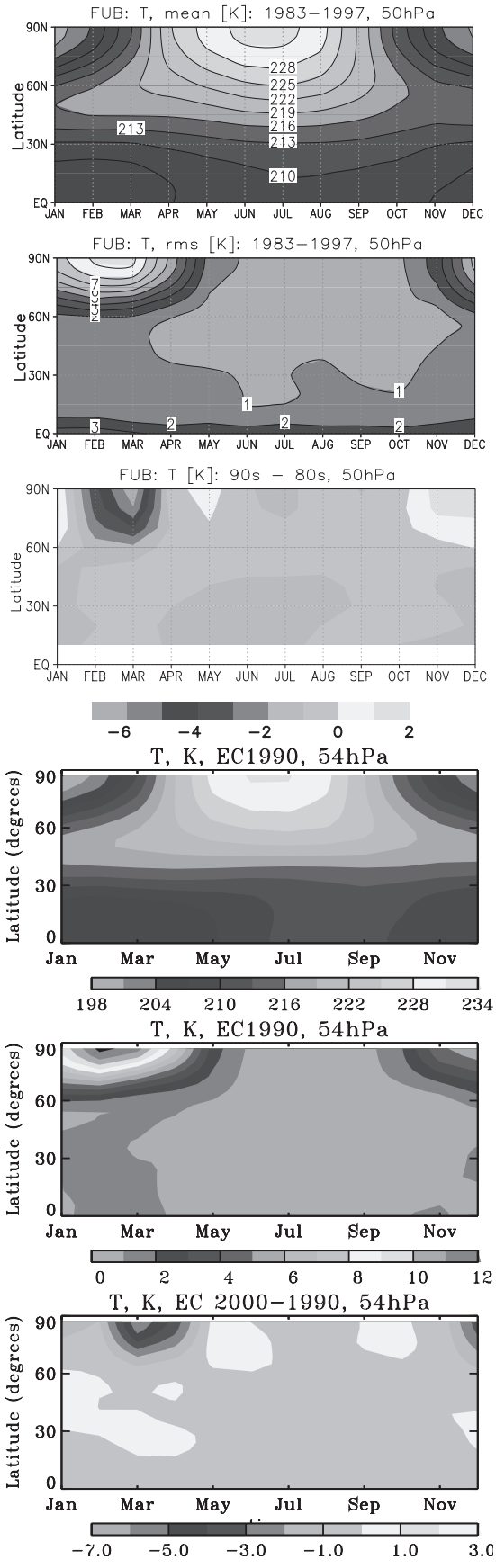

separated by the minima at the vortex edge and the subtropical barriers, represented in the left panel of Figure 7 by the latitude regions with steep gradients in the mixing ratio. However, the mixing ratios are systematically shifted to lower values, as it occurs also in other models [*Douglass et al.*, 1999].

[32] Analysis of potential vorticity by *Manzini and Feichter* [1999] shows also that MA-ECHAM4 reproduces strong gradients at the subtropical barriers. This is supported also by comparison with CRISTA data discussed in more detail in section 8.

[33] The residual mean circulation of the MA-ECHAM4-CHEM model has been included in the intercomparison of *Austin et al.* [2002]. For the Northern Hemisphere, December–January–February period, their Figure 7 shows that the MA-ECHAM4-CHEM stream function compares well with that deduced from the ECMWF reanalysis (ERA15). This means that the downward motion of air through the 50 hPa level in the Northern polar cap is realistic in the MA-ECHAM4-CHEM model, consistent with a good simulation of the average temperature there. Given that downwelling in the Arctic winter stratosphere drives the tropical upwelling [*Holton et al.*, 1995], the strength of the latter should be reasonably realistic. As Figure 8 demonstrates, the model reproduces important features of the observed vertical propagation of the seasonal signal in tropical water vapor, the so-called "tropical tape recorder" [*Mote et al.*, 1998]. Figure 8 depicts the deviations of the water vapor mixing ratios from the 6-year mean at each altitude in a latitude belt between 5S and 5N both for observations and model. Selecting a larger latitude range of ±15 degrees gives a somewhat smoother picture especially for the HALOE data but does not change the main structures. The model also captures the semiannual oscillation (SAO) in the mesosphere and upper stratosphere. From closer scrutiny it appears that the model's vertical transport is too fast between about 100 and 50 hPa (as discussed for other models by *Douglass et al.* [1999]) and too slow between 40 and 10 hPa. From the observed H_2O distribution a mean upward vertical velocity in the 100 to 10 hPa region of the tropics of about 0.3–0.4 mm/s is estimated. In the model this is in average about 0.5–0.6 mm/s, but 0.8 mm/s near 100 hPa and only 0.1–0.2 mm/s at 30 hPa, the latter acting as a bottleneck for vertical transport of source gases like methane or nitrous oxide (see also Figure 6). Compared to the residual vertical velocity derived from observations and radiation by *Rosenlof et al.* [1997] the values calculated by the model are low by almost a factor of 2 between 40 and 7 hPa which might explain the low bias in methane and nitrous oxide. The too fast vertical propagation of the water signal below 50 hPa might be not related to transport but to overestimated dehydration by overshooting convective

Figure 4. (opposite) Upper 3 panels: Free University of Berlin observations, monthly and zonal average mean temperatures and standard deviations for 1983–1997 and mean differences between the periods 1991–2000 and 1981–1990, lower 3 panels: temperature statistics calculated by MA-ECHAM for the 1990 scenario and mean differences between the two scenarios; all data approximately for the 50 hPa level in the Northern Hemisphere.

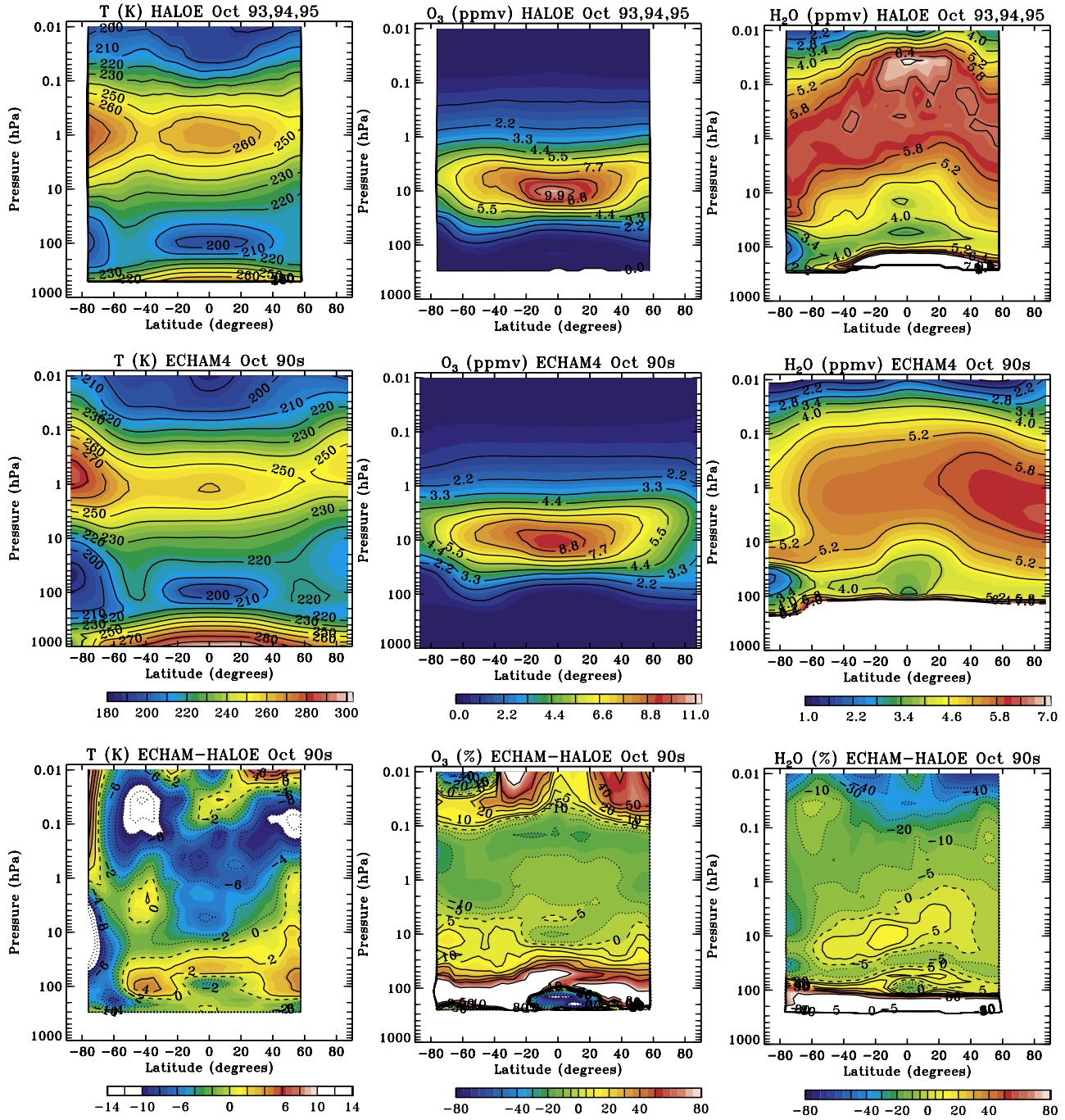

Figure 5. Zonal average temperature (left), ozone (middle) and water vapor (right) calculated by the MA-ECHAM model (average of 20 Octobers, middle row) compared to observations by the satellite instrument HALOE (average of October 1993 to 1995, top panels), including absolute and percentage differences (lower panels).

clouds and a cold bias at 70 hPa near the equator in northern hemispheric early spring (seen in analysis of snapshots). However, influence of numerical artifacts from the advection scheme as discussed by *Gregory and West* [2002] cannot be excluded. The model does not reproduce the QBO which might be another reason for the underestimate of vertical transport at 30 – 20 hPa, as indicated by sensitivity studies with a new version of the model with much better vertical resolution and simulated QBO [*Giorgetta et al.*, 2002].

[34] In order to assess the role of interactive chemistry (e.g., prognostic ozone) on the variability of the stratosphere, an additional simulation has been performed with the MAECHAM4 model without the CHEM chemistry module and instead a prescribed climatological ozone distribution. The prescribed ozone climatology is the monthly zonal mean ozone presented by *Fortuin and Kelder* [1998]. It is based on ozonesonde observations (1000–10 hPa) and SBUV-SBUV/2 satellite data in the stratosphere (30–0.3 hPa), and covers the 1980–1991 decade. Therefore

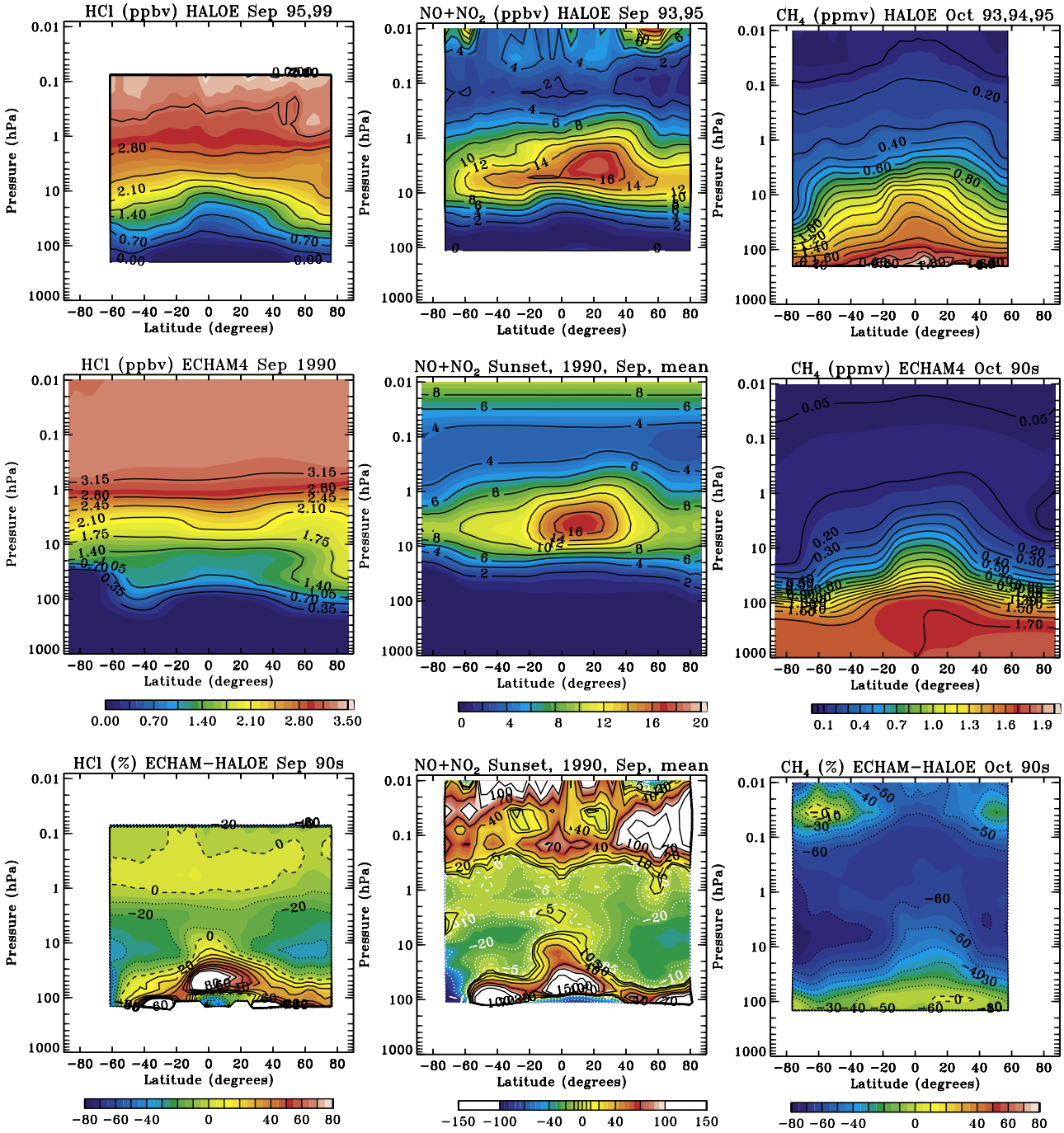

Figure 6. Zonal average of HCl (left), NOx (middle) (averages 20 Septembers) and CH_4 (averages of 20 Octobers, right) from the MA-ECHAM model (middle row) compared to observations by HALOE (top row, HCl average of September 1995 and 1999, NO + NO_2 average of September 1993 and 1995, and CH_4 average of October 1993 to 1995). Model data for NO_x at sunset are sampled in the same scanning pattern as the satellite data. Lower panels percentage differences. The large differences in the troposphere are mostly due to uncertain HALOE-data and to be ignored.

the prescribed ozone includes the early years of the ozone hole development. In the simulation without CHEM, the greenhouse gases are specified for typical 1990 conditions and the climatological sea surface temperature (average 1979–1989; GISS-HADLEY, see Table 1) are used. Results are reported from a 20-year simulation after spin up.

[35] Figure 9 depicts the relationship between January–February eddy heat fluxes (at 100 hPa) and March temperature (at 50 hPa) in the lower stratosphere, following *Newman et al.* [2001]. The variability in the eddy heat flux is a measure of the dynamical activity arising from meteorological disturbances in the troposphere and it is not particularly affected by interactive chemistry: Both models show eddy heat fluxes ranging from 10 to 20 Km/s, in good agreement with the heat fluxes diagnosed from the NCEP reanalysis. For a detailed discussion of the NCEP results, see *Newman*

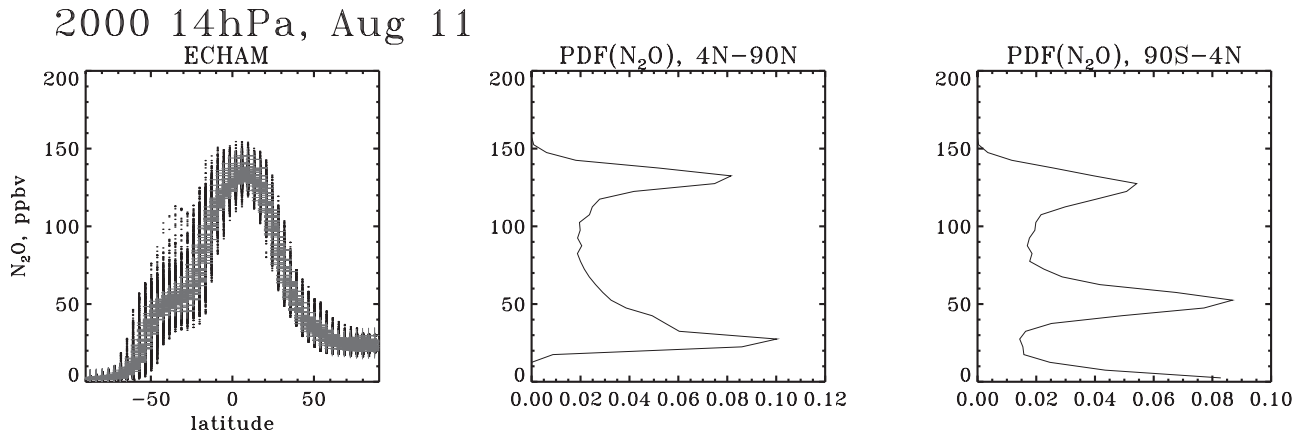

Figure 7. N_2O at 14 hPa: left: Individual data points at all longitudes for 20 realizations of 11 August as function of latitude, zonal means in dark gray, middle: area weighted probability density functions of mixing ratio bins north of 4N (summer hemisphere), right: same south of 4N (winter hemisphere). 2000 scenario (1990 scenario similar), compare to *Sparling* [2000].

et al. [2001]. The March temperature response to the heat fluxes is also comparable within the two models and with respect to the NCEP reanalysis. Only for very weak heat fluxes does the model with interactive chemistry tend to induce colder temperatures. This sensitivity results in a change of the slope of the regression line from 0.84 for the model without chemistry to 1.3 from the model with interactive chemistry and of the intercept temperature (measure of the radiative equilibrium temperature) from 204 K to 195 K, respectively. Presumably, at low heat fluxes (relatively unperturbed dynamic conditions) the radiative-chemical feedback between ozone depletion and temperature [*Shine*, 1986] does play a role in the model with interactive chemistry in lowering the March temperature. Note that the NCEP data range from 1979 to 1999, therefore it includes years with reported ozone depletion only for the last decade (for instance 1997, the open box at (11 Km/s, 207 K)). Given that both simulations are for fixed conditions, it is not unexpected that the regression lines differ somewhat between each simulation and the observations.

[36] Figure 10 (upper panel) depicts the daily and interannual variability associated with sudden stratospheric warming at 30 hPa. Clearly the level of dynamical activity is comparable in the two models at the North Pole, because of the dominant role played by planetary waves in determining the temperature in the polar winter and spring stratosphere. A similar behavior is found also lower down at 70 hPa. Consistent with these findings, there is no

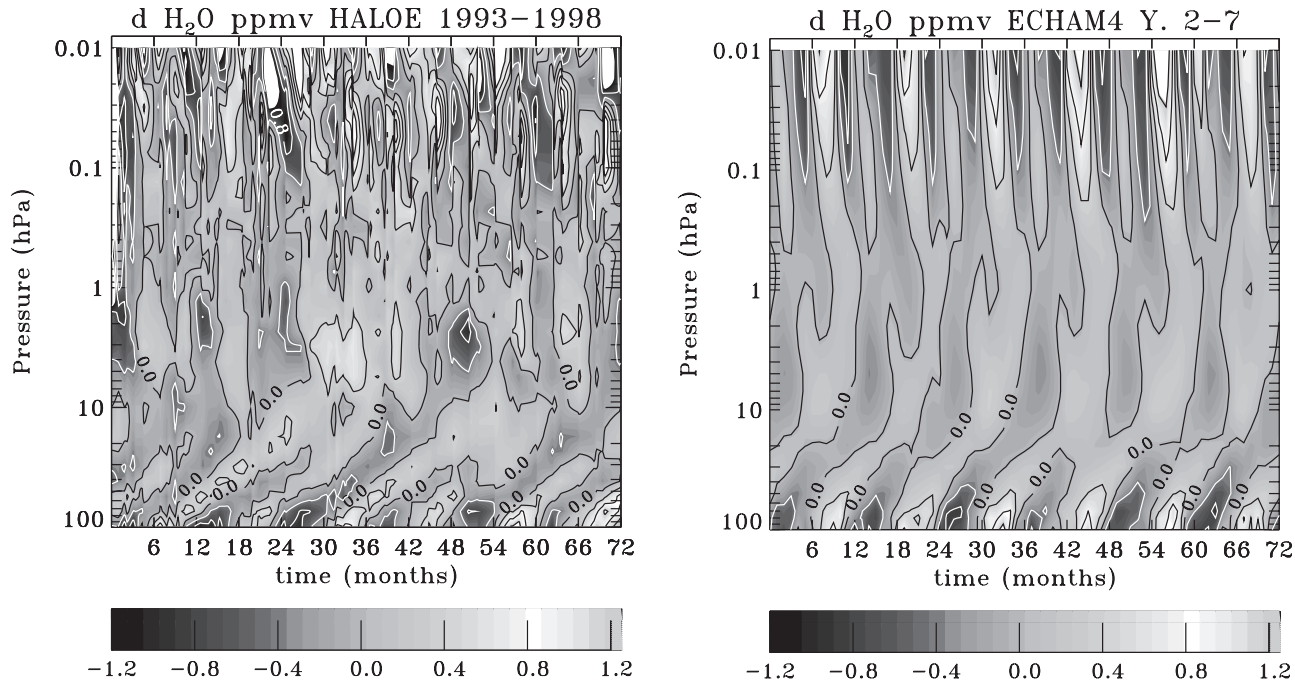

Figure 8. The "tropical tape recorder" in stratospheric water vapor observed by HALOE (left), and modelled by MA-ECHAM (right). Shown are the concentration differences from the six-year mean at the different altitudes in a latitude bin between 5S and 5N.

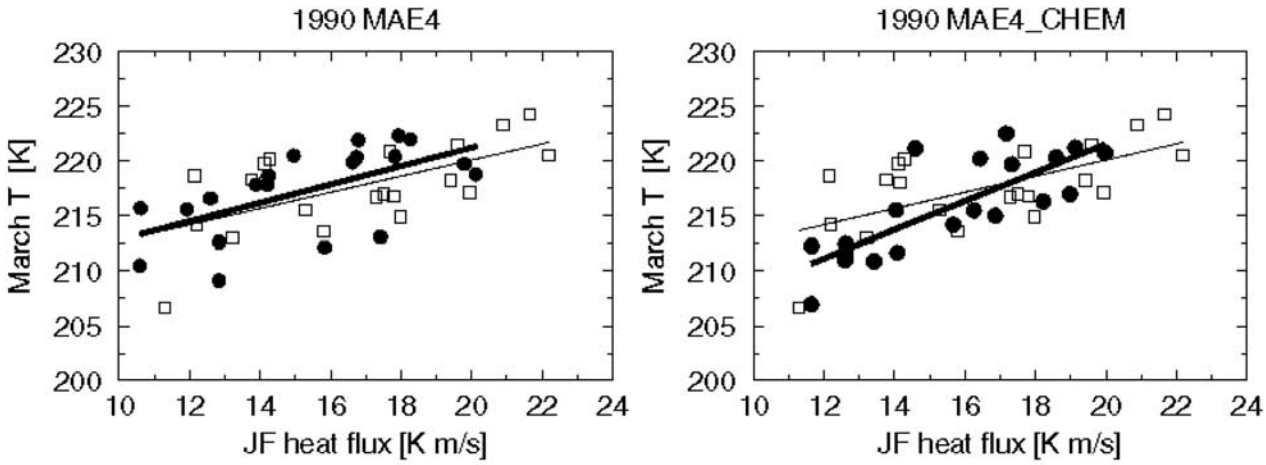

Figure 9. Scatter plot of the January–February meridional heat flux at 100 hPa (40 N–80 N average) and the March temperature at 50 hPa (60 N–90 N average). Each symbol is an individual year. Black circles, thick line: Model results, no chemistry at left and with interactive chemistry at right. Open squares, thin line: NCEP meteorological re-analysis (1979 to present).

statistically significant difference in the average temperatures in the North polar lower stratosphere (see the upper panel of Figure 11).

[37] At the South Pole instead (Figure 11 lower panel), there is a statistically significant shift to colder temperature (from 5 to 10 K in October and between 10 and 14 K in November) in the average temperature. Concerning daily and interannual variability, Figure 10 (lower panel) shows that both models are characterized by much less variability in the Southern polar region (with respect to the Northern polar region). For both models the variability is confined to the spring season, a realistic behavior although variability at the beginning of the spring could be underestimated because of the model cold bias in the upper stratosphere. The comparison between the two model suggests an enhancement of the interannual (but not daily) variability in October, November and December in the model with interactive chemistry (e.g., wider temperature excursions for the red curves with respect to the black curves). Presumably, the temperature interannual variability is larger in the interactive model because low ozone in dynamically quiet years feeds back to produce additional cooling.

[38] In summary, for the climate and chemical composition typical of 1990, the positive radiative-dynamical feedback between ozone depletion and temperature does play a role in determining the average temperature and the polar interannual variability in the Southern Hemisphere during spring, while the Northern Hemisphere is dominated by the dynamical forcing, except at very low heat fluxes.

[39] Feedback between chemistry and dynamics is also important in the upper stratosphere for performing trend studies as will be shown in part 2 [*Manzini et al.*, 2003] where the change from near past to present is evaluated.

6. Lower Stratosphere in Spring of Both Hemispheres: Statistics

[40] The largest chemical dynamical feedbacks occur at slightly higher altitudes in the Northern Hemisphere than in

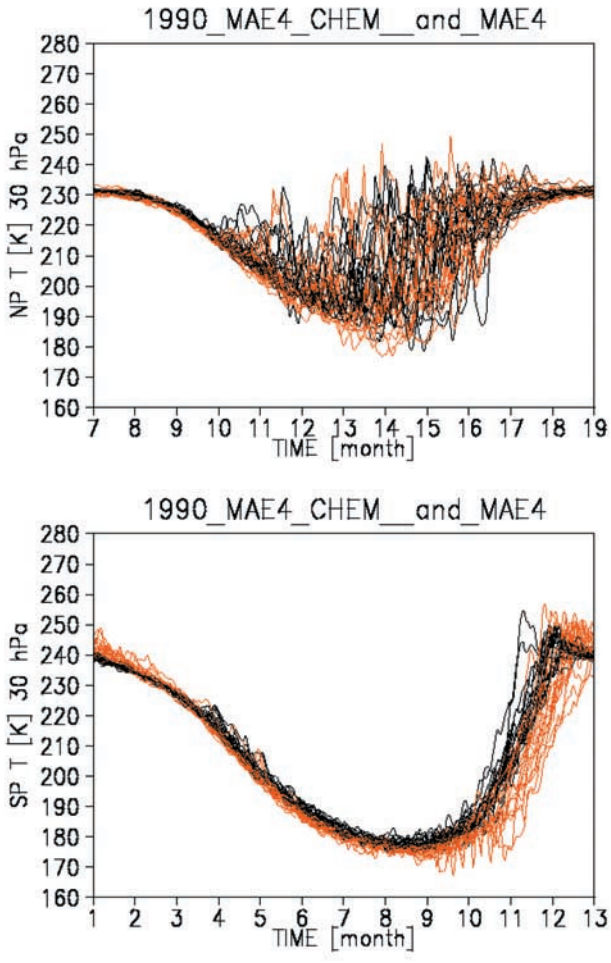

Figure 10. Daily North (upper) and South (lower) Pole temperature at 30 hPa. Black: from the 20 years simulation with the model without chemistry. Red: from the 20 year simulation with the model that includes interactive chemistry.

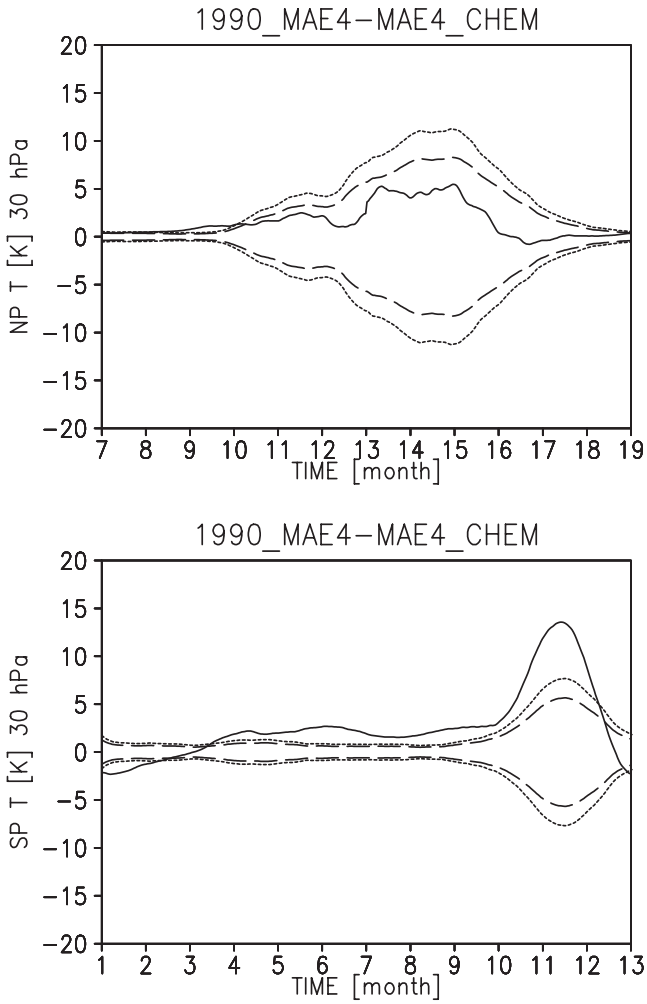

Figure 11. 20 year ensemble average of the 31-day running mean temperature differences (without - with interactive chemistry) at 30 hPa at the poles. The dashed (dotted) curve is the envelope outside which the difference is significant at the 95% (99%) level.

the Southern Hemisphere. In northern hemispheric spring the 50 hPa level is selected for analysis because for this level long-term compilations of radiosonde data are available and because around this level heterogeneous chemical ozone depletion is most significant in observations (e.g., *Hofmann and Deshler* [1991], HALOE data of spring 1993, 1995, 1996, 1997, 2000). Figure 12 shows 20 year averages of temperatures for March for the late nineties obtained with the model together with FU Berlin observations. For both, model and observations, the coldest region is located northeast of Scandinavia and the warmest near the Bering Strait. For both periods (early nineties not shown) the model agrees with the data within about 3 K, the temperature difference between the cold and warm centers being larger in the model. In the data as well as the model the cold region, slightly west of the most likely position of the

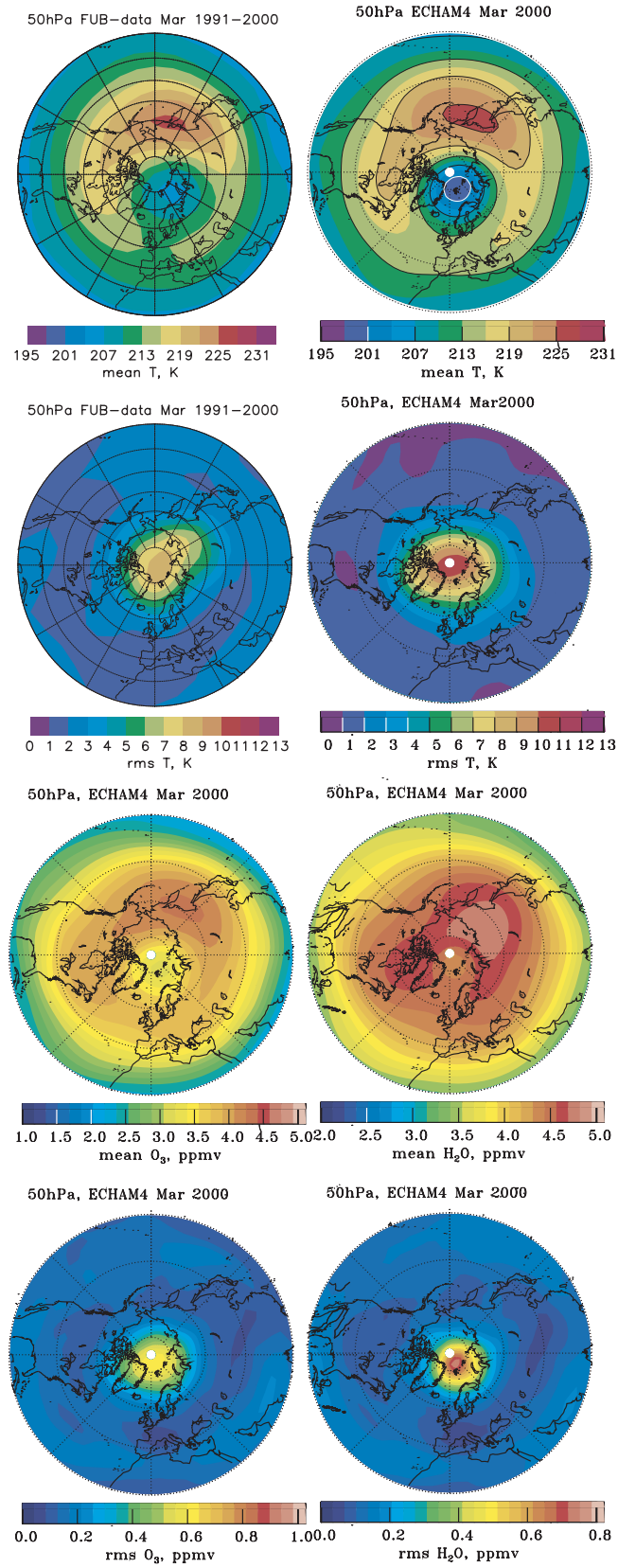

Figure 12. (opposite) Observed March mean temperatures and standard deviations (rms) for the period 1991 to 2000 (upper left) at 50 hPa as compiled by Free University of Berlin (stereographic projection) compared to the simulations with MA-ECHAM4 for late nineties (upper right). Lower four panels mean and standard deviation of calculated ozone and water vapor.

vortex, exhibits lower temperatures for the conditions of the late nineties compared to the early nineties (see also Figure 4). The largest variability in temperature (rms) occurs near the pole, mostly related to variations in vortex strength and position, and sudden stratospheric warmings. The model variability near the pole is larger than in the observations, reflecting the occasional occurrence of too cold or too warm springs. In the model the variability and its difference from observations is somewhat larger for the early nineties scenario.

[41] The cold region coincides with a region of reduced ozone and enhanced water vapor with slight reduction in the center from occasional dehydration, typical for vortex air, as can be seen from Figure 12. The region of largest variability is shifted off the pole to the most likely position of the vortex, the region where feedbacks between chemistry and dynamics are most important.

[42] In the southern spring the mean values are more zonally symmetric. In Figure 13 October averages for the 70 hPa level, the level with the most pronounced chemical feedbacks, are shown. Ozone and temperatures near the South Pole are very low, as well as water vapor because of significant dehydration by PSCs. Near the vortex center, the model is about 3–4 K colder than the UKMO analysis of temperature observations. A pronounced ozone and water vapor maximum is found south of Australia which coincides with a temperature maximum in the UKMO analysis for the years 1992–1999. The modelled patterns of temperature standard deviations mostly agree with the observations. The largest simulated variability of ozone occurs near the vortex edge adjacent to the midlatitude maximum, whereas the largest variability of water vapor occurs near the vortex center as well at the edge near the east Antarctic coast.

[43] In both hemispheres the positive feedback between ozone and temperature, via radiative heating and PSC chemistry, appears to be important. In the Southern Hemisphere it is strongest in November while in the Northern Hemisphere it is more pronounced in April than in March.

[44] Note that in lower latitudes the variability of water vapor and ozone is larger in northern spring than in southern spring.

7. Lower Polar Stratosphere: Polar Stratospheric Clouds and Interannual Variability

[45] Since heterogeneous chemistry is strongly nonlinear in temperature and chlorine concentrations we focus in this section on snapshots of extreme cases in observations and simulations of the year 2000 time slice. Interannual variability in the model is due to internal variability of the model dynamics.

7.1. Water Vapor, HNO_3, and Polar Stratospheric Clouds

[46] Differences in water vapor mixing ratios in the Arctic and Antarctic stratosphere have a significant impact on heterogeneous ozone depletion. The model results agree well with satellite observations, at least at the 70 hPa and 50 hPa levels which are most important for ozone. At higher altitudes in the Antarctic winter and spring dehydration is overestimated because of the model's cold bias. Figure 14 presents one example showing the effects of dehydration in

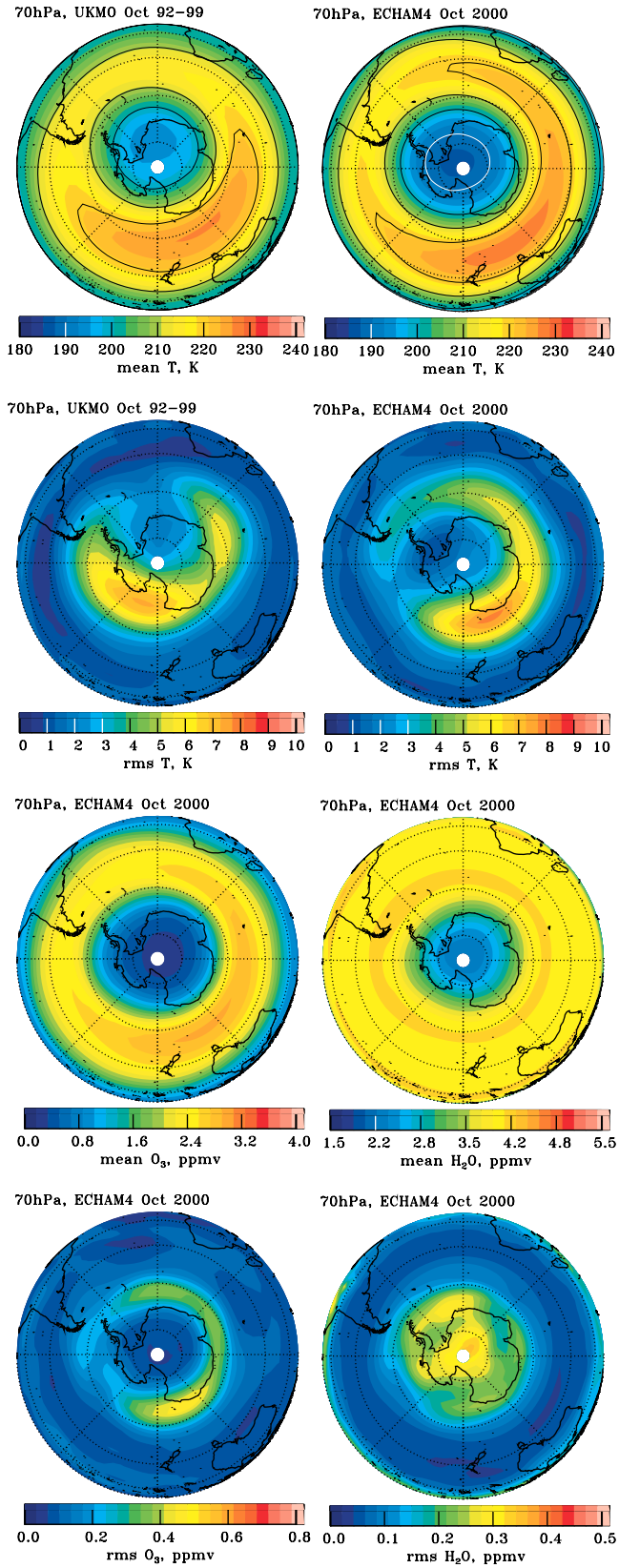

Figure 13. Observed temperature mean and standard deviation for October 1991–2000 (UKMO) in the Antarctic (upper left) and 20 yrs mean and standard deviations of the 2000 time slice of MA-ECHAM for temperature (upper right), ozone and water vapor (lower panels) at 70 hPa. Orthographic projection.

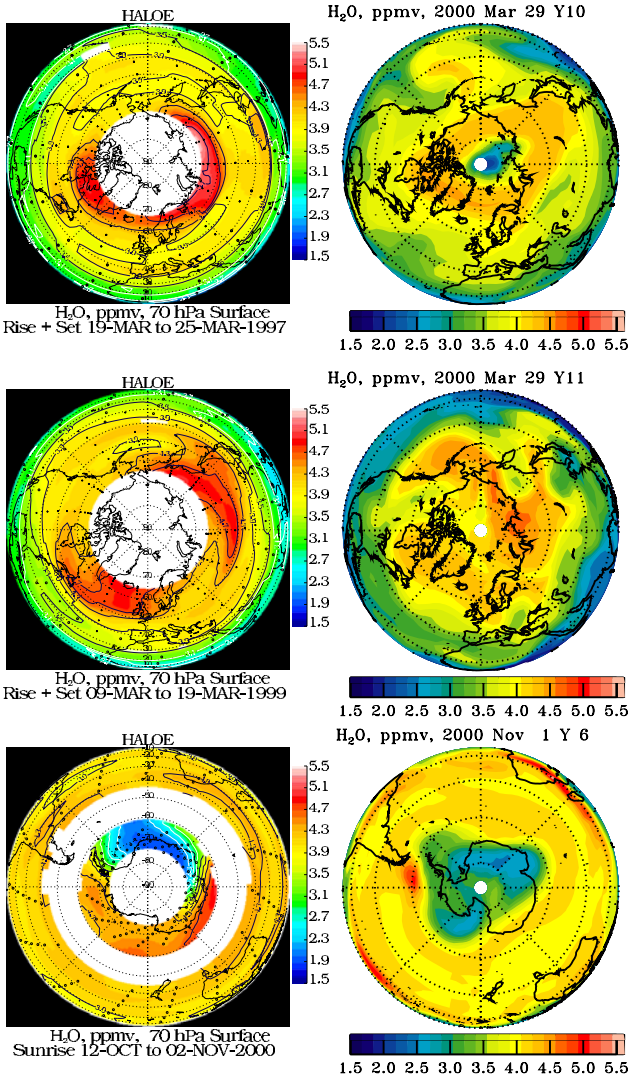

Figure 14. Snapshots of water vapor at 70 hPa: Left: HALOE observations. Right: MA-ECHAM. First row: cold Arctic spring (29 March), second row: warm Arctic spring, third row: Antarctic spring (1 November). The selected model years correspond to the following subsection.

Antarctica and two examples in the Arctic, indicating H_2O enhancements in the vortex or vortex remnants due to downward transport. In the Antarctic the observed interannual variability and the mean concentrations are reproduced by the model. In the Arctic, modeled water vapor appears to be low by about 10%, consistent with the underestimated methane transport to the upper stratosphere. Also dehydration in cold years appears to be overestimated, however, HALOE observations in very high latitudes are not available and other observations are sparse. Observations by the ILAS satellite [*Pan et al.*, 2002] indicate that in the Arctic significant dehydration is possible, even around 25 km, where it appears also sometimes in the model.

[47] Another important quantity for simulation of PSCs is nitric acid vapor. Calculated HNO_3 in late October and early November in the Southern Hemisphere is close to the MLS-observations at the 50 to 100 hPa levels (70 hPa shown in Figure 15) indicating that HNO_3 transport by sedimentation of particles during winter and spring is well reproduced, also since we obtain good agreement in early winter (June, not shown, see *Santee et al.* [1999]). The underestimate at 70 hPa in midlatitudes is associated with the deficiencies in upward transport of N_2O (see above and section 8) so that insufficient NO_y is produced in the middle atmosphere. In the Arctic during spring the underestimate of HNO_3 due to the N_2O transport deficit in the tropics is more pronounced above about 60 hPa. Denitrification in the cold part of the vortex at 70 hPa due to formation of NAT and settling of particles is clearly visible in the MLS observations as well as the model results. In 1995, the observed longitudinal variability is less than in 1996 shown in Figure 15. Furthermore, the interannual HNO_3 variability in the model is quite strong, with the highest values in warm springs, similar to the observations compiled by *Santee et al.* [1999]. The maximum calculated value at 70 hPa is more than 10% lower than the maximum in the observations for March 1996.

[48] Regarding the representation of denitrification by particle settling, even the simple assumption that sedimenting ice particles carry HNO_3 downward yields reasonable results for the Antarctic lower stratosphere. For the Arctic this simplification sometimes causes an underestimate of denitrification since selective growth of NAT particles is not

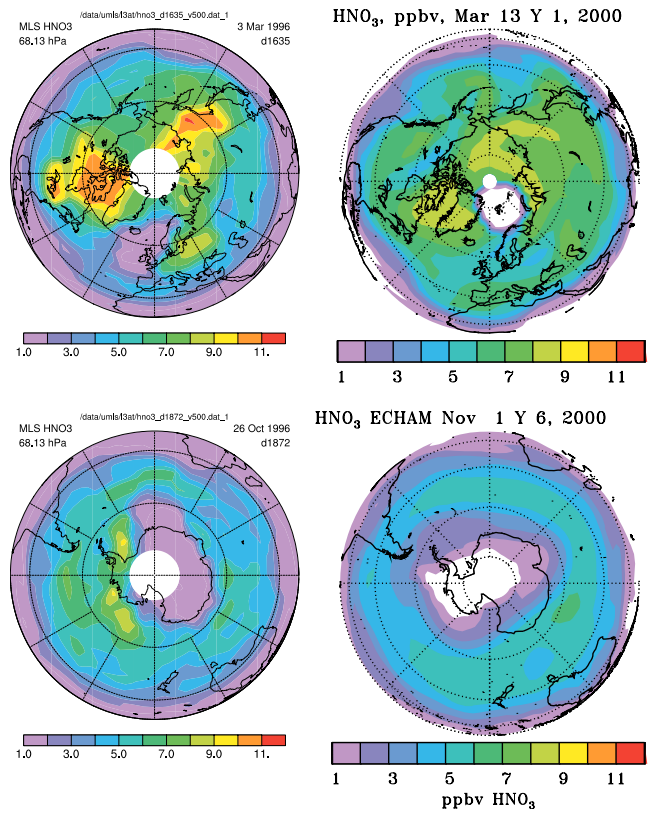

Figure 15. Snapshots of HNO_3 vapor at 70 hPa: left: observations by MLS on UARS, right: MA-ECHAM. Upper panels Arctic spring (3 March 1996 for MLS and 13 March for the model), lower panels Antarctic spring (26 October 1996 for MLS and 1 November for model). In the left panels mixing ratios of less than 1 ppb are still blue, but not in right ones.

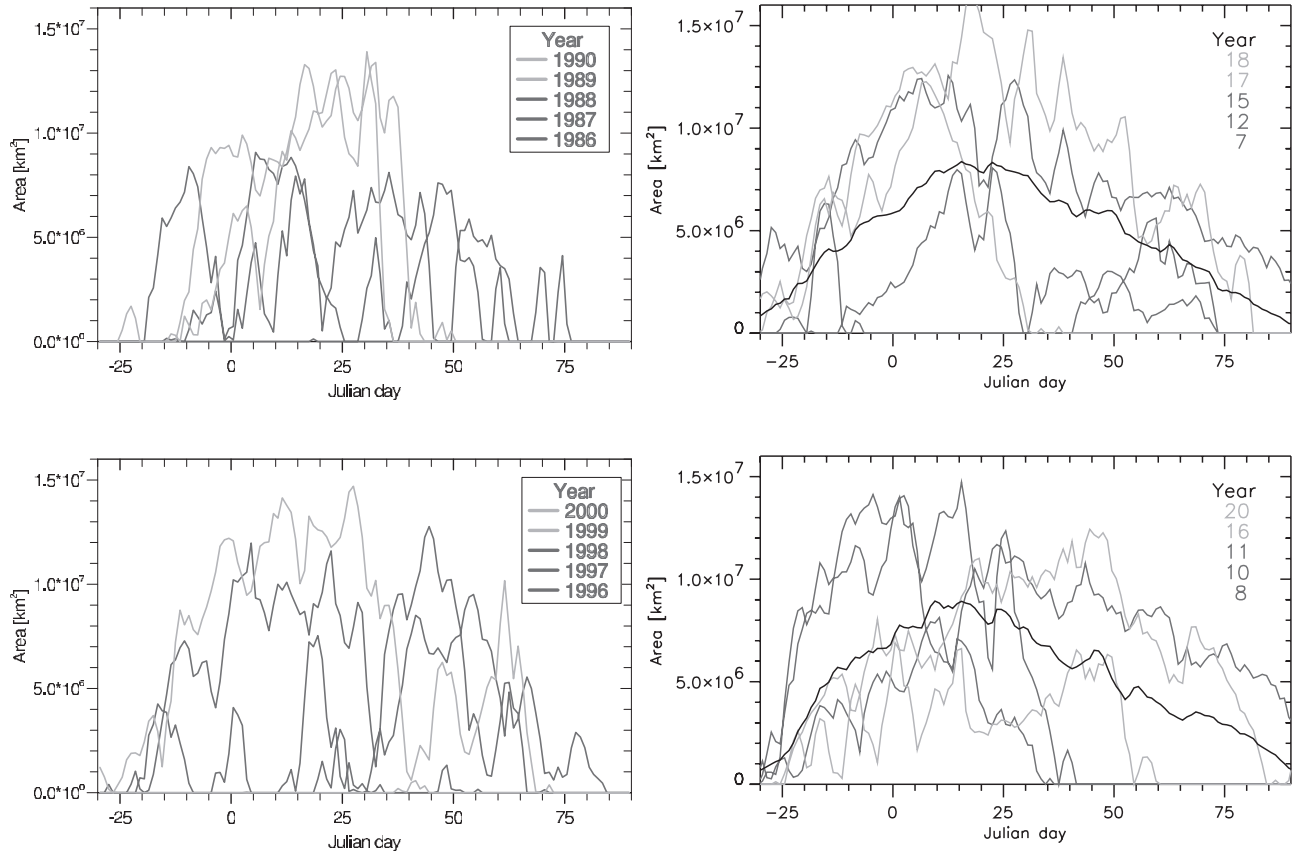

Figure 16. Examples of area covered with PSCs at 54 hPa in the Northern Hemisphere for 40 winters as calculated by MA-ECHAM (right panels) compared with 10 years of observations at the 475 K surface compiled by G. Braathen, NILU, Norway (presented on a poster at the EGS-Assembly in Nice, 2001; left panels). The black line in the model panels represents the 20 years average of each time slice (top 1990, bottom 2000).

considered [e.g., *Fahey et al.*, 2001]. However, in very cold model years settling of ice particles causes denitrification which leads to enhanced ozone depletion so that in the average calculated ozone is close to observations. Problems with the cold bias at 30 hPa in the Antarctic have been reduced by assuming a larger particle number density, leading to smaller particles and a reduced settling velocity.

[49] Figure 16 shows the area covered by PSCs at about 50 hPa for a representative subset of the 40 Arctic model winters and PSCs diagnosed from observations from the last two decades as compiled by G. Braathen of NILU. The model reproduces the interannual variability in mid-winter and early spring. The mean areal coverage is overestimated by about 20%. The model tends to overestimate the PSC area in March in cold winters because of an occasional cold bias at about 30 hPa and a consequently too persistent vortex. In Antarctica the cold bias allows PSCs to persist until the first weeks of November, i.e., about 2 weeks longer than observed before 2001 (see below). The vortex area and its variability agrees with observations.

7.2. Chlorine Partitioning and Ozone Depletion

[50] In this section we focus on the polar lower stratosphere in spring, when a combination of heterogeneous chemistry, radiative heating and dynamical processes determines the ozone and temperature distributions. Results for both the Antarctic and Arctic regions are presented. Given that the natural interannual variability (e.g., strength of the vortex, extremes in the polar temperature, distortions of the polar vortex by planetary waves) is large in the lower stratosphere during spring, polar orthographic maps are shown for a number of months, representative of the range of conditions both simulated and observed. It cannot be expected that the selected snapshots represent all the details in the observations. We have selected typical conditions from the model results and observations to study if significant features are simulated by the free running model.

[51] In Antarctica in November the feedback processes between temperature and ozone [*Randel and Wu*, 1999; *Waugh et al.*, 1999] are strongest. In September ozone in the model is high-biased compared to the observations because of too high ozone values in winter (see section 5.1 and 5.2) and because bromine chemistry as been neglected (minor effect). Observed and modelled ozone holes peak in early October, being very similar in depth, but delayed by about a week in the model. Subsequently, in late November or December the vortex breaks up. The timing of the circulation change is controlled to a large extent by the solar heating by ozone, which can be delayed

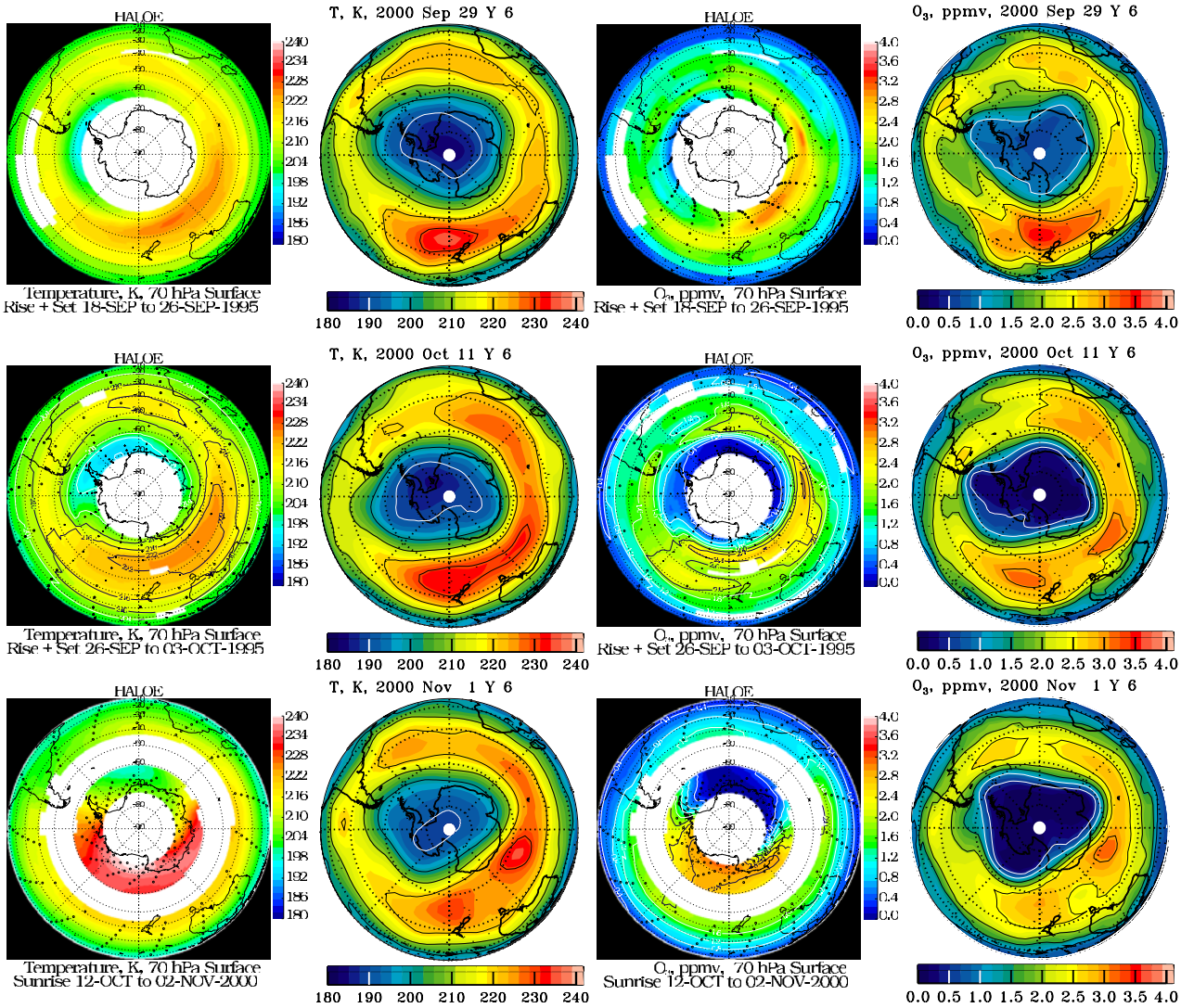

Figure 17. Snapshots of temporal development of temperature and ozone at 70 hPa in Antarctic spring: first column: temperature observations by NCEP/HALOE, second column: computed temperature by MA-ECHAM, model year 6, boundary conditions for 2000. Third column: observed O_3, last column: computed O_3. HALOE observes at the highest latitudes at 18 September, 3 October, and 2 November, symbols mark data points, model output is for 29 September, 11 October, and 1 November. White spots indicate data gaps.

by persisting ozone destruction in the presence of polar stratospheric clouds. The interannual variability is largely associated with planetary wave activity excited in the troposphere.

[52] The polar orthographic Antarctic maps in Figure 17 depict the temporal development of temperature and O_3 fields at 70 hPa during Austral spring for two selected years of HALOE observations and a typical model year out of the 20 years of simulation for the conditions of the late nineties. The HALOE observations at high latitudes represent late September, early October and early November, the model fields are snapshots for individual days of the year 2000 time slice. The associated results for ClO_x, HCl and $ClONO_2$ are shown in Figure 18. As a consequence of the HALOE occultation technique and the large variability due to fast chemistry and strong horizontal gradients, the observations in high latitudes are only representative for a period of about 3 days, so that it would not be useful to compare with monthly means here. It can be seen from Figure 17 that the model captures the main features of temperature and ozone distributions. Low temperatures are correlated with low ozone values within the polar vortex. In the model ozone depletions lag the observations by about 10 days. Because of the model cold bias of about 2 K in the polar lower stratosphere, in most of the 40 years of simulation PSCs are still present in early November, maintaining chlorine in its ozone depleting form, ClO_x, so that HCl concentrations are low in some parts of the vortex, as shown in Figure 18. PSCs at this time of the year were recently observed from the POAM satellite instrument [*Bevilacqua and the POAM Team*, 2002], which is able to cover very high latitudes not in the range of HALOE or other UARS instruments. In regions where ozone is low and/or the temperature is above the PSC threshold, HCl increases

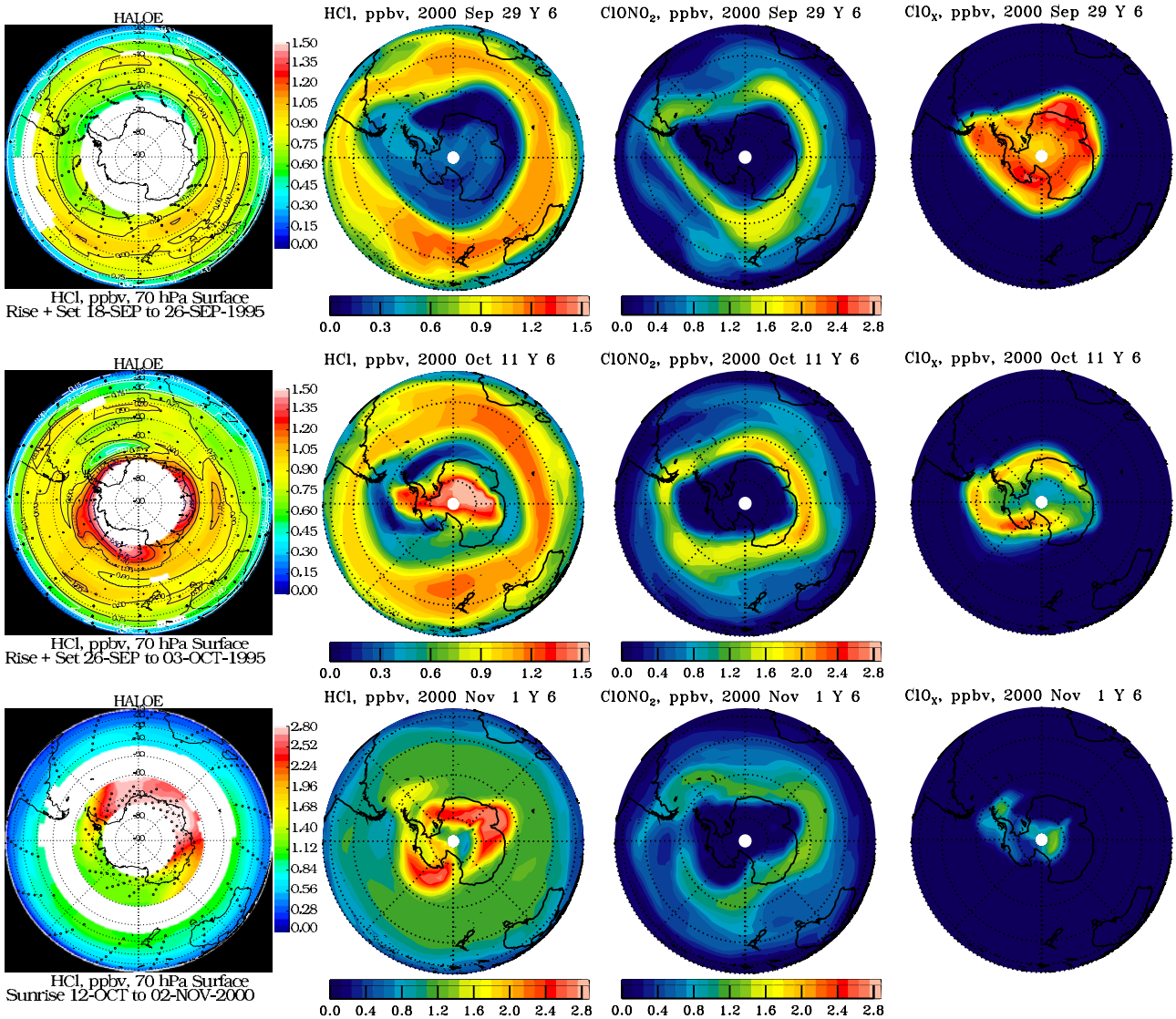

Figure 18. As Figure 17 but observed HCl (first column) and modelled chlorine partitioning (second to fourth column), Antarctica. ClOx = ClO + $2Cl_2O_2$ + ClOH (reactive chlorine). Note the enhanced scale for the four HCl panels in the upper left.

rapidly in agreement with the observations. In the cold springs this happens with a delay of up to about two weeks. In the 2000 time slice the increase of HCl occurs earlier than in the 1990 time slice because of faster ozone depletion related to higher total inorganic chlorine. $ClONO_2$ remains low inside the vortex and forms a "collar" at the vortex edge as also seen by CLAES on UARS (*Roche et al.* [1994] and J. Mergenthaler (personal communication, 2001)). Since CLAES operated only in a period strongly perturbed by Pinatubo, we performed a short sensitivity run with strongly enhanced stratospheric sulfate aerosol in which the model $ClONO_2$ was still higher than the observations although within the uncertainty range and with similar patterns.

[53] In the Arctic where the vortex is often shifted off the pole, March is most interesting because efficient ozone destruction is possible with the return of sunlight. In addition, feedback processes involving PSCs can be very efficient. Polar orthographic temperature and ozone maps at 70 hPa are shown in Figure 19, for three years of HALOE data covering late March and three snapshots for 29 March of selected model years of the 2000 time slice. The examples represent a cold and a warm spring and a situation at vortex breakup after a cold winter. Two of these years are also shown in Figure 16. Figure 19 indicates that the observed interannual variability in Arctic spring temperatures is reproduced by the model, although the model tends to be slightly too cold. One has to take into account, however, that the coldest regions are not observed by HALOE, especially in the cold spring of 1997 where the minimum in the HALOE-data near the vortex edge is as high as 201 K while in the center 190–192 K has been observed (ECMWF-data). A warm spring like 1998 is simulated as well (model year 11). Ozone is depleted if the temperature is sufficiently low, with the best example in model year 10 where the final vortex breakup occurred as late as early May, very similar to the situation in 1997 (or concerning ozone depletion, 1996 and

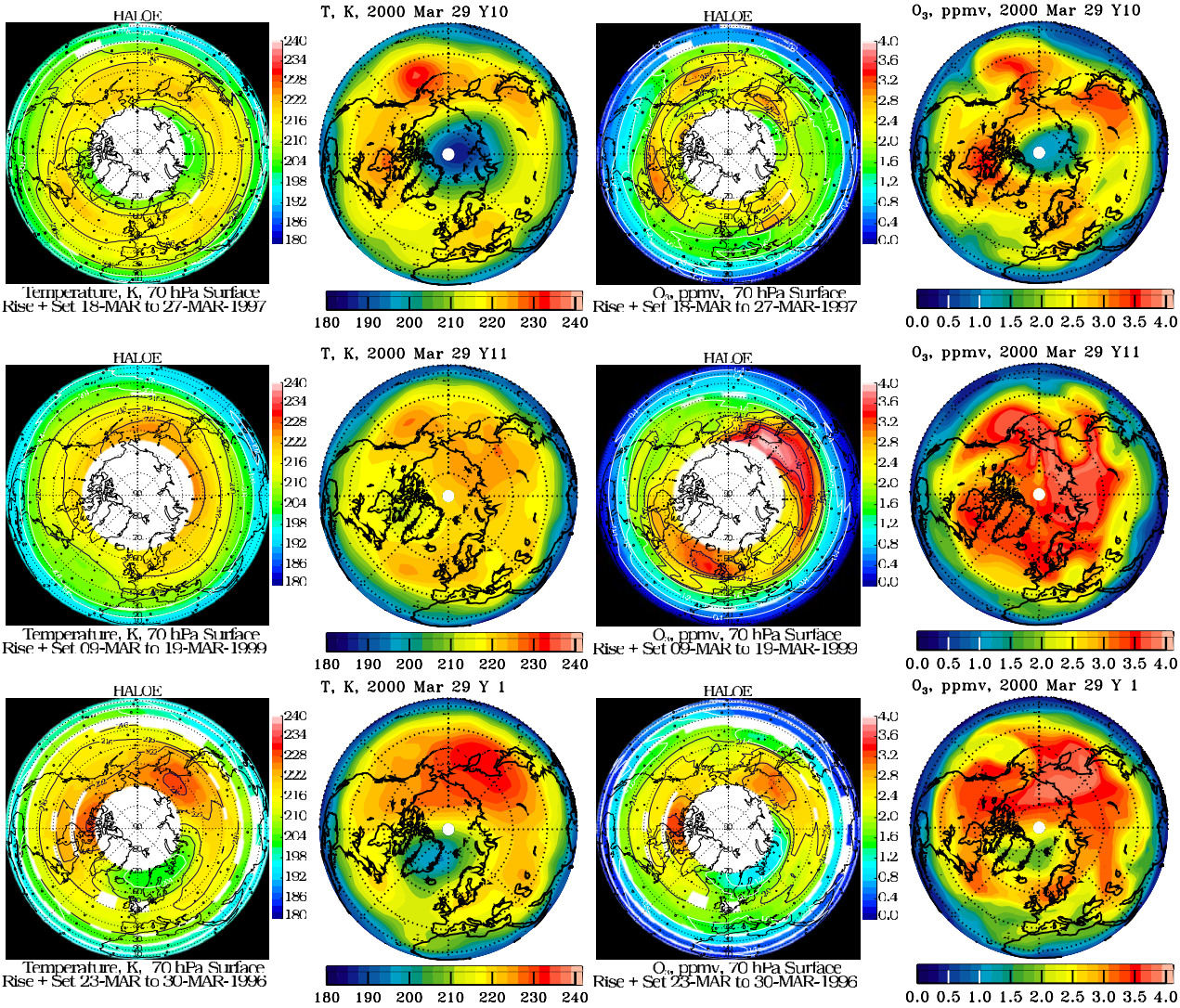

Figure 19. Snapshots of temperature and ozone at 70 hPa in Arctic spring. First column: temperature observations by NCEP/HALOE; second column: computed temperature by MA-ECHAM, model years 10, 11, 1, boundary conditions for 2000; third column: observed O_3; last column: computed O_3. First row: cold and stable vortex; second row: warm spring; third row: at vortex breakup after a cold winter. HALOE observes at the highest latitudes at 27 March, 19 March, and 30 March, symbols mark data points, model output is for 29 March.

2000). In Figure 19 simulated ozone at middle and high latitudes is about 10% too high, resulting from the overestimate of transport from the tropical production region. Except for this bias the model agrees well with the observations. This includes advection of ozone-poor low-latitude air over the Atlantic (1996 and model years 10 and 1) and the strong polar-centered vortex in 1997 (to be compared with model year 10).

[54] As in Antarctica, in cold springs, model PSCs tend to be too persistent (Figure 16) which maintains low levels of HCl. Cases of low HCl have been observed in late March of 1997 and early March of 2000, see Figure 20, depicting HCl fields from the HALOE-data. Calculated ClO_x in cold winters is consistent with MLS observations of ClO [*Santee et al.*, 1996a, 2000]. The re-formation of $ClONO_2$ in the vortex in spring (especially in model year 1) agrees well with CLAES-observations [*Santee et al.*, 1996b] as shown in Figure 20 (ClO_x and $ClONO_2$ from the simulation). The model reproduces the interhemispheric differences in the chlorine partitioning in the spring vortex, with typically slowly increasing HCl in the Arctic and rapid HCl reformation in Antarctic.

8. Discussion

[55] The circulation and temperature at high latitudes during winter are known to be influenced by the simulated strength of the momentum deposition due to gravity waves. Given that this process is parameterized, an implicit uncertainty in its contribution to momentum and energy fluxes of the middle atmosphere cannot be avoided. An estimate of the sensitivity of the middle atmosphere circulation as simulated by the MA-ECHAM4 model (without interactive chemistry) to the specification of the gravity wave source

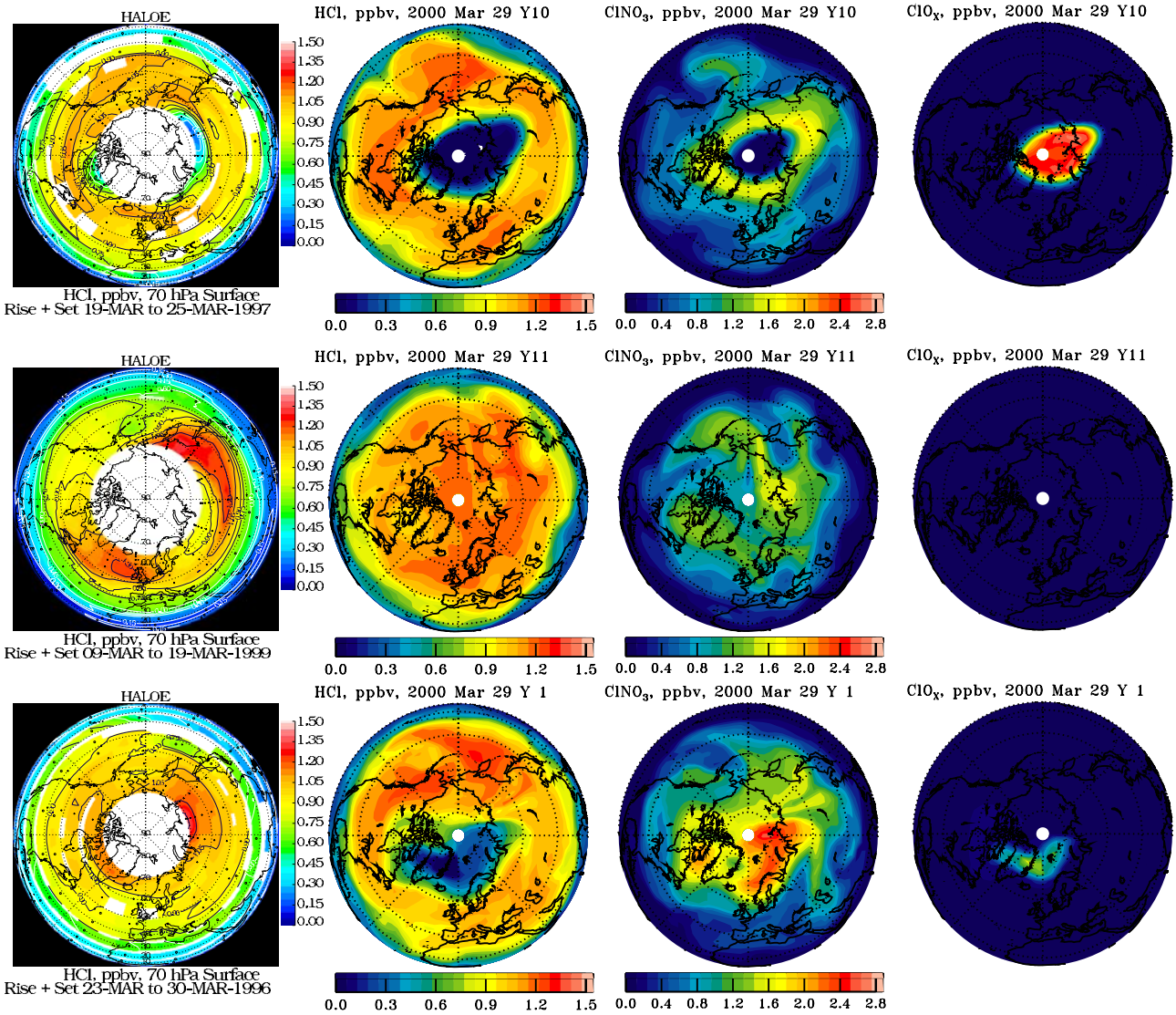

Figure 20. As Figure 19 but observed HCl (first column) and calculated chlorine partitioning (second to fourth column), Arctic. ClOx = ClO + $2Cl_2O_2$ + ClOH (reactive chlorine).

spectrum is given by *Manzini and McFarlane* [1998]. They have shown that in principle it is possible to virtually eliminate the polar winter cold bias if seasonal and geographical variability of the gravity wave source spectrum are specified within reasonable bounds. However, it is still an open question how exactly to specify the gravity wave source spectrum, because observational and theoretical knowledge on generation and statistics of gravity waves are lacking (e.g., hemispherical and seasonal differences). The specifications of the gravity wave parameterization used in the current simulation are based on the model version without interactive chemistry, no further tuning is done. This might have some effect in Antarctic spring. In a comparison of 13 GCMs by *Pawson et al.* [2000] MA-ECHAM was the closest to observations for Northern Hemisphere, for the Southern Hemisphere it belonged to the better half.

[56] In the simulations for 1990 and 2000 there are one and three years, respectively, where in the model denitrification occurs via formation and sedimentation of ice particles in the Arctic. Dehydration and denitrification via ice has been observed also during the SOLVE-campaign. The sedimentation of so-called NAT-rocks [*Fahey et al.*, 2001] is not present in our PSC scheme. Nevertheless the simulated denitrification and dehydration does not appear to be unrealistic in both hemispheres compared to observations.

[57] With respect to the tropical middle atmosphere, comparison with the HALOE water vapor data has shown a realistic semiannual water vapor variation at the stratopause. At the stratopause, the semiannual variations in the water vapor deviations are driven by the semiannual oscillation in zonal wind that is simulated successfully in the MA-ECHAM4 model [*Manzini et al.*, 1997]. Work is in progress to alleviate the QBO problem known to be related to a number of factors, including insufficient vertical and horizontal resolutions and deficiencies in the generation of vertically propagating waves that force the QBO (for implications of an assimilated QBO, see *Giorgetta and Bengtsson* [1999]; for a high-resolution version, *Giorgetta el al.* [2002]).

[58] Numerical inconsistencies in the model influence the simulation. A principal problem is the transformation from the spectral domain for the meteorological equations to the (vertical) hybrid grid for the rest of processes. This causes inconsistencies in surface pressure or total mass that effects the transport across the tropopause [*Jöckel et al.*, 2001]. On the other hand, the spectral method used by the dynamical component of the model requires a different representation of the dynamical fields than that required by the SPITFIRE transport algorithm. For example the winds and mass fields are specified at cell centers for the dynamical model, while SPITFIRE requires the normal component of each wind fields specified at the cell walls. The dynamical component of the model uses a combination of centered and semi-implicit finite differences for the time stepping algorithm. SPITFIRE is a forward-in-time two time level algorithm. These differences, especially concerning the vertical wind component, a small quantity derived from the large horizontal components by a diagnostic equation, can generate inconsistencies in the simulation [*Segers et al.*, 2002; *Bregman et al.*, 2002]. We have tried to reduce these problems; however, further improvements are still possible by implementing the methods of the three references above. The ideal solution would be to use the same algorithm and variable representations for the model dynamics and tracer transport algorithms.

[59] As mentioned in previous work [e.g., *Eluszkiewicz et al.*, 2000; *Gregory and West*, 2002; *Rotman et al.*, 2001, Figures 3 and 4] the choice of the advection scheme significantly influences the calculated tracer distributions. During the development stage test runs with the semi-Lagrangian transport scheme (SLT) [*Rasch and Williamson*, 1990; *Rasch et al.*, 1995] have been performed. With SLT the upward transport in the lower stratosphere is better and stratosphere-troposphere exchange is reduced. On the other hand, the downward transport in the polar vortices as well as the horizontal gradients at the vortex edges are strongly underestimated by the SLT scheme, preventing the formation of a realistic ozone hole. The faster upward transport in the tropical lower stratosphere is due to the large numerical diffusion in SLT schemes which causes unrealistic age of air [e.g., *Eluszkiewicz et al.*, 2000]. Note that the tendencies of its mass fixer needed to compensate for the violation of mass conservation common to SLT-schemes, are as large as the advection tendencies. Therefore conclusions from modeled tracer distributions on middle atmospheric dynamics have to be drawn with some caution.

[60] It is interesting to note that the present model (at T30 resolution) reproduces tongue-like features in the middle stratosphere, the "streamers" in the subtropics and mid-latitudes, as observed by the CRISTA-instrument [*Riese et al.*, 1999] on the Space Shuttle in November 1994 and August 1997. Figure 21 shows ozone at 10 hPa in model year 15 as an example. Positions of streamers and gradients of ozone are close to those observed in both hemispheres. The streamers occur frequently also in the other 19 model years; their variability is related to the shape and strength of the polar vortices (indicated by the violet regions in Figure 21). They are also apparent in the distributions of HNO_3 and long-lived source gases like N_2O and $CH4_4$

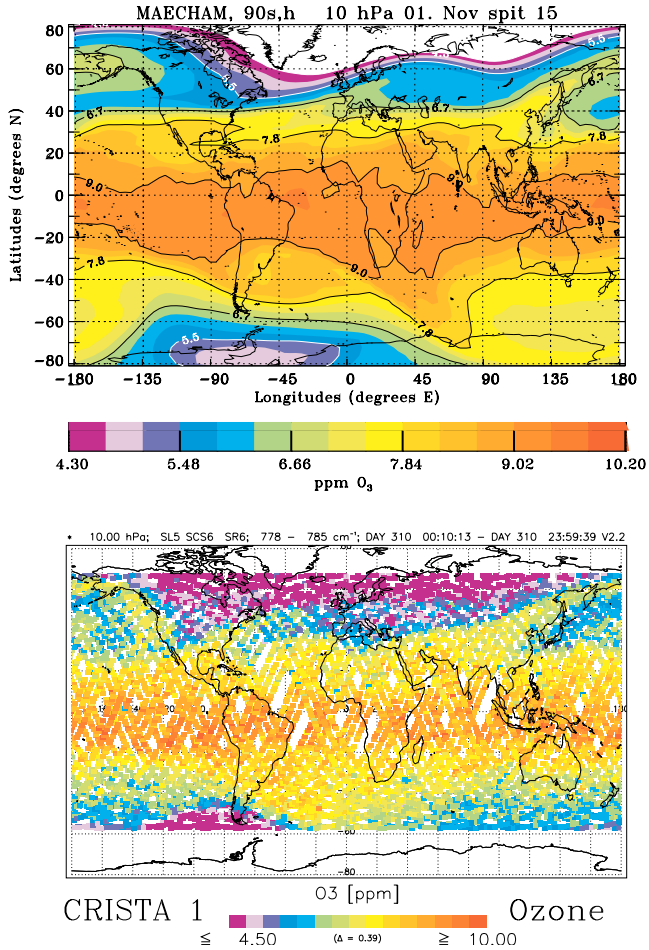

Figure 21. "Streamers" in ozone at 10 hPa in the MA-ECHAM model (upper panel, here model year 15) and observed by the Space-Shuttle instrument CRISTA [*Riese et al.*, 1999] in November 1994 (lower panel).

down to about 50 hPa as observed. All the comparisons with CRISTA show also that the model reproduces the gradients at the subtropical barriers. Below about 50 hPa an increase in horizontal and vertical resolution might improve the simulation of the subtropical barrier (see also Figure 6). The SPITFIRE advection scheme is essential to maintain the strong gradients along the "streamers"; with the more diffusive semi-Lagrange scheme of the standard ECHAM4 model these structures are unrealistically smooth (with our resolution).

[61] For future model versions it is planned also to include bromine chemistry. Furthermore, the scheme for polar stratospheric clouds will be refined, mostly following *Waibel et al.* [1999]. This will also consider liquid ternary particles, and allow for two classes of solid NAT particles with different number concentrations [*Fahey et al.*, 2001] to improve the representation of denitrification in the Arctic. As discussed by *Solomon* [1999] and *Santee et al.* [1999], denitrification only plays a minor role in the Arctic for present conditions, but might be more important in future scenarios because of climate feedbacks [*Waibel et al.*, 1999]. Our simulations in the subsequent parts of this paper and simulations by other groups [*Austin et al.*,

2002] indicate however that a cooling of the arctic lower stratosphere due to greenhouse gases is unlikely.

9. Summary and Conclusions

[62] MA-ECHAM4-CHEM interactively combines a middle atmosphere GCM with a chemical model, including most of the important reactions and species necessary to describe the stratospheric, lower mesospheric, and tropospheric chemistry. It is nevertheless computationally fast enough to allow long-term integrations with currently available computer resources. Comparison with 9 years of data from the Upper Atmosphere Research Satellite and other observations has shown that the model runs without drifts for decades and is able to reproduce the most important features of the dynamics and chemistry of the stratosphere and lower mesosphere. This holds for the zonal and monthly mean values of temperatures and ozone and the most important chemically active species, as well as their spatial and temporal variability. Feedbacks between chemistry and atmospheric physics are most important in the polar vortices in late spring and contribute to the large interannual variability, especially in the Northern Hemisphere. In the tropical lower stratosphere with interactive chemistry the mean upwelling is enhanced compared to the off-line model, but nevertheless the mean vertical transport is too small to capture observed distributions of source gases like methane and nitrous oxide. The problem might be partially related to vertical and horizontal resolution and the missing QBO. For the quasi-steady-state time slice experiments the resulting biases in NO_x, Cly and water vapor due to the above transport deficiencies are in the order of 10% i.e., small enough for realistic sensitivity studies.

[63] Dehydration, denitrification and chlorine partitioning in the polar vortices by heterogeneous chemistry closely reproduce observations, including interhemispheric differences. The model is very sensitive to relatively small changes in chlorine concentrations between the early and late nineties (to be discussed in more detail in part 2). Ozone depletion in high-latitude spring is delayed by a few days in both hemispheres, most likely because of high-biased ozone concentrations in midwinter due to deficiencies in dynamics. In the upper stratosphere ozone and water vapor, interactively calculated by the chemical module and the radiative heating scheme, produce temperatures in agreement with observations. During winter, the polar night temperature throughout the middle atmosphere is to a large extent controlled by breaking and dissipation of planetary waves in the stratosphere and gravity waves in the mesosphere. The associated wave induced driving of the mass circulation in the model realistically reproduces the resulting downward transport of chemical tracers into the polar vortex.

[64] **Acknowledgments.** We thank James Russell of Hampton University and the HALOE team at NASA/Langley, Hampton, Virginia, for support in using HALOE data, Michelle Santee of NASA/JPL, Pasadena, California, and John Mergenthaler of Lockheed Martin Research Laboratory, Palo Alto, California, for providing figures of MLS and CLAES data, and Peter Preusse and Friedhelm Olschewski of CRISTA team at University of Wuppertal for the CRISTA figures. We also thank L. Bengtsson, G. P. Brasseur, M. A. Giorgetta, and H. Schmidt at Max-Planck-Institute for Meteorology in Hamburg for discussion and for reading the manuscript and suggesting constructive comments, and U. Schlese and U. Schulzweida there and at DKRZ for technical assistance. The development of this model was mostly funded by the German Research Ministry for Education and Research (BMBF) in the framework of the Ozone Research Program and AFO2000 (KODYACS and MEDEC). The computations were performed at the Max-Planck-Institute for Meteorology on a NEC SX-4; UKMO data were taken from the SPARC database.

References

Austin, J., A three-dimensional coupled chemistry-climate model simulation of past stratospheric trends, *J. Atmos. Sci.*, *59*, 218–232, 2002.

Austin, J., J. R. Knight, and V. Butchart, Three dimensional chemical model simulations of the ozone layer: 1979–2015, *Q. J. R. Meteorol. Soc.*, *126*, 1533–1556, 2000.

Austin, J., et al., Assessments of chemistry-climate models of the stratosphere, *Atmos. Chem. Phys. Discuss.*, *2*, 1035–1096, 2002.

Bacher, A. J. M. Oberhuber, and E. Roeckner, ENSO dynamics and the seasonal cycle in the tropical Pacific as simulated by the ECHAM4/OPIC3 coupled general circulation model, *Clim. Dyn.*, *14*, 431–450, 1998.

Barath, F. T., et al., The Upper Atmosphere Research Satellite Microwave Limb Sounder Instrument, *J. Geophys. Res.*, *98*, 10,751–10,762, 1993.

Bengtsson, L., E. Roeckner, and M. Stendel, Why is the global warming proceeding much slower than expected?, *J. Geophys. Res.*, *104*, 3865–3876, 1999.

Bevilacqua, R., and the POAM Team, The Polar Ozone and Aerosol Measurement (POAM II and III) experiments: An overview of observations of polar ozone and related constituents and phenomenology, paper presented at Assembly of the European Geophysical Society, Nice, France, 2002.

Bey, I., D. J. Jacob, R. M. Yantosca, J. A. Logan, B. D. Field, A. M. Fiore, Q. Li, H. Y. Liu, L. J. Mickley, and M. G. Schultz, Global modeling of tropospheric chemistry with assimilated meteorology: Model description and evaluation, *J. Geophys. Res.*, *106*, 23,073–23,095, 2001.

Bregman, B., A. Segers, M. Krol, E. Meijer, and P. van Velthoven, On the use of mass-conserving wind fields in chemistry-transport models, *Atmos. Chem. Phys. Discuss.*, *2*, 1765–1790, 2002.

Brühl, C., and P. J. Crutzen, NO_x-catalyzed ozone destruction and NO_x activation at midlatitudes to high latitudes as a main cause of the spring to fall ozone decline in the Northern Hemisphere, *J. Geophys. Res.*, *105*, 12,163–12,168, 2000.

Brühl, C., et al., Halogen Occultation Experiment ozone channel validation, *J. Geophys. Res.*, *101*, 10,217–10,240, 1996.

Brühl, C., K. Carslaw, T. Peter, J.-U. Grooß, J. M. Russell III, and R. Müller, Chlorine activation and ozone depletion in the arctic vortex of the four recent winters using a trajectory box model and HALOE satellite observations, in *Atmospheric Ozone: Proceedings of the Quadrennial Ozone Symposium 1996*, vol. 2, edited by R. D. Bojkov and G. Visconti, pp. 675–667, Int. Ozone Comm., Geneva, 1998a.

Brühl, C., K. Carslaw, and T. Peter, Ozone depletion in the Arctic vortex of winter 1996/97 using HALOE data and a chemical boxmodel on real and idealized trajectories, in *Polar Stratospheric Ozone 1997*, edited by N. Harris, I. Kilbane-Dawe, and G. T. Amanatidis, *Air Pollut. Res. Rep. 66*, pp. 253–256, Eur. Commun., Brussels, 1998b.

Brühl, C., P. J. Crutzen, and J. U. Grooß, High-latitude, summertime NO_x activation and seasonal ozone decline in the lower stratosphere: Model calculations based on observations by HALOE on UARS, *J. Geophys. Res.*, *103*, 3587–3597, 1998c.

Cariolle, D., A. Lassere-Bogorry, J. F. Royer, and J. F. Geleyn, A general circulation model simulation of the spring time Antarctic ozone decrease and its impact on mid-latitudes, *J. Geophys. Res.*, *95*, 1883–1898, 1990.

Carslaw, K. S., T. Peter, and S. L. Clegg, Modeling the composition of liquid stratospheric aerosols, *Rev. Geophys.*, *35*, 125–154, 1997.

Colella, P., and P. R. Woodward, The piecewise parabolic method (PPM) of gas-dynamical simulations, *J. Comput. Phys.*, *54*, 174–200, 1984.

Crutzen, P. J., and C. Brühl, Catalysis by NO_x as the main cause of the spring to fall stratospheric ozone decline in the Northern Hemisphere, *J. Phys. Chem. A*, *105*, 1579–1582, 2001.

Crutzen, P. J., and U. Schmailzl, Chemical budgets of the stratosphere, *Planet. Space Sci.*, *31*, 1009–1032, 1983.

Dameris, M., V. Grewe, R. Hein, C. Schnadt, C. Bruhl, and B. Steil, Assessment of the future development of the ozone layer, *Geophys. Res. Lett.*, *25*, 3579–3582, 1998.

Douglass, A. R., M. J. Prather, T. M. Hall, S. E. Strahan, P. J. Rasch, L. C. Sparling, L. Coy, and J. M. Rodriguez, Choosing meteorological input for the global modeling initiative assessment of high-speed aircraft, *J. Geophys. Res.*, *104*, 27,545–27,564, 1999.

Drdla, K., and R. P. Turco, Denitrification through PSC formation: A 1-D model incorporating temperature oscillations, *J. Atmos. Chem.*, *12*, 318–366, 1991.

Eckman, R. S., W. L. Grose, R. E. Turner, and W. T. Blackshear, Polar ozone depletion: A three-dimensional chemical modeling study of its long-term global impact, *J. Geophys. Res.*, *101*, 22,977–22,989, 1996.

Eluszkiewicz, J., R. S. Hemler, J. D. Mahlmann, L. Bruhwiler, and L. L. Takacs, Sensitivity of age-of-air calculations to the choice of advection scheme, *J. Atmos. Sci.*, *57*, 3185–3201, 2000.

Fahey, D. W., et al., The detection of large HNO_3-containing particles in the winter Arctic stratosphere, *Science*, *291*, 1026–1031, 2001.

Fortuin, J. P., and H. Kelder, A ozone climatology based on ozondesonde and satellite measurements, *J. Geophys. Res.*, *103*, 31,709–31,734, 1998.

Giorgetta, M. A., and L. Bengtsson, The potential role of the quasi-biennial oscillation in the stratosphere-troposphere exchange as found in water vapour in general circulation model experiments, *J. Geophys. Res.*, *104*, 6003–6019, 1999.

Giorgetta, M. A., E. Manzini, and E. Roeckner, Forcing of the quasi-biennial oscillation from a broad spectrum of atmospheric waves, *Geophys. Res. Lett.*, *29*(8), 1245, doi:10.1029/2002GL014756, 2002.

Gregory, A. R., and V. West, The sensitivity of a model's stratospheric tape recorder to the choice of advection scheme, *Q. J. R. Meteorol. Soc.*, *128*, 1827–1846, 2002.

Grooß, J.-U., R. Müller, G. Becker, D. S. McKenna, and P. J. Crutzen, The upper stratospheric ozone budget: An update of calculations based on HALOE data, *J. Atmos. Chem.*, *34*, 171–183, 1999.

Hall, T. M., D. W. Waugh, K. A. Boering, and R. A. Plumb, Evaluation of transport in stratospheric models, *J. Geophys. Res.*, *104*, 18,815–18,839, 1999.

Hanson, D. R., and K. Mauersberger, Laboratory studies of nitric acid trihydrate: Implications for the south polar stratosphere, *Geophys. Res. Lett.*, *15*, 855–858, 1988.

Haynes, P. H., C. J. Marks, M. E. McIntyre, T. G. Shepherd, and K. P. Shine, On the "downward control" of extratropical diabatic circulations by eddy-induced mean zonal forces, *J. Atmos. Sci.*, *48*, 651–678, 1991.

Hein, R., et al., Results of an interactively coupled atmospheric chemistry-general circulation model: Comparison with observations, *Ann. Geophys.*, *19*, 435–457, 2001.

Hervig, M. E., et al., Validation of temperature measurements from the Halogen Occultation Experiment, *J. Geophys. Res.*, *101*, 10,277–10,286, 1996.

Hines, C. O., Doppler spread parameterization of gravity wave momentum deposition in the middle atmosphere. Part 1: Basic formulation, *J. Atmos. Sol. Terr. Phys.*, *59*, 371–386, 1997a.

Hines, C. O., Doppler spread parameterization of gravity wave momentum deposition in the middle atmosphere. Part 2: Broad and quasi monochromatic spectra and implementation, *J. Atmos. Sol. Terr. Phys.*, *59*, 387–400, 1997b.

Hofmann, D. J., and T. Deshler, Evidence from balloon measurements for chemical depletion of stratospheric ozone in the Arctic winter of 1989-90, *Nature*, *349*, 300–305, 1991.

Holton, J. R., P. H. Haynes, M. E. McIntyre, A. R. Douglass, R. B. Rood, and L. Pfister, Stratosphere-troposphere exchange, *Rev. Geophys*, *33*, 403–439, 1995.

Jöckel, P., R. von Kuhlmann, M. G. Lawrence, B. Steil, C. A. M. Brenninkmeijer, P. J. Crutzen, P. J. Rasch, and B. Eaton, On a fundamental problem in implementing flux-form advection schemes for tracer transport in 3-dimensional general circulation and chemistry transport models, *Q. J. R. Meteorol. Soc.*, *127A*, 1035–1052, 2001.

Landgraf, J., and P. J. Crutzen, An efficient method for online calculations of photolysis and heating rates, *J. Atmos. Sci.*, *55*, 863–878, 1998.

Leonard, B. P., M. K. MacVean, and A. P. Lock, The flux integral method for multidimensional convection and diffusion, *Appl. Math. Model.*, *19*, 333–342, 1995.

Leonard B. P., A. P. Lock, and M. K. MacVean, Conservative explicit unrestricted-time-step multidimensional constancy-preserving advection schemes, *Mon. Weather Rev.*, *124*, 2588–2606, 1996.

Lin, S. J., and R. Rood, Multi-dimensional flux-form semi-Lagrangian transport schemes, *Mon. Weather Rev.*, *124*, 2046–2070, 1996.

Mahowald, N. M., R. A. Plumb, P. J. Rasch, J. del Corral, F. Sassi, and W. Heres, Stratospheric transport in a three-dimensional isentropic coordinate model, *J. Geophys. Res.*, *107*(D15), 4254, doi:10.1029/2001JD001313, 2002.

Manzini, E., and H. Feichter, Simulation of the SF_6 tracer with the middle atmosphere MAECHAM4 model: Aspects of the large-scale transport, *J. Geophys. Res.*, *104*, 31,097–31,108, 1999.

Manzini, E., and N. A. McFarlane, The effect of varying the source spectrum of a gravity wave parameterization in a middle atmosphere general circulation model, *J. Geophys. Res.*, *103*, 31,523–31,539, 1998.

Manzini, E., N. A. McFarlane, and C. McLandress, Impact of the Doppler spread parameterization on the simulation of the middle atmosphere circulation using the MA/ECHAM4 general circulation model, *J. Geophys. Res.*, *102*, 25,751–25,762, 1997.

Manzini, E., B. Steil, C. Brühl, M. A. Giorgetta, and K. Krüger, A new interactive chemistry-climate model: 2. Sensitivity of the middle atmosphere to ozone depletion and increase in greenhouse gases: Implications for recent stratospheric cooling, *J. Geophys. Res.*, *108*, doi:10.1029/2002JD002977, in press, 2003.

McFarlane, N. A., The effect of orographically exited gravity drag on the general circulation of the lower stratosphere and troposphere, *J. Atmos. Sci.*, *44*, 1775–1800, 1987.

Mote, P. W., T. J. Dunkerton, M. E. McIntyre, E. A. Ray, P. H. Haynes, and J. M. Russell, Vertical velocity, vertical diffusion, and dilution by midlatitude air in the tropical lower stratosphere, *J. Geophys. Res.*, *103*, 8651–8666, 1998.

Newman, P. A., E. R. Nash, and J. E. Rosenfield, What controls the temperatures of the Arctic stratosphere during the spring?, *J. Geophys. Res.*, *106*, 19,999–20,010, 2001.

Pan, L. L., W. J. Randel, H. Nakajima, S. T. Massie, H. Kanzawa, Y. Sasano, T. Yokota, T. Sugita, S. Hayashida, and S. Oshchepkov, Satellite observation of dehydration in the Arctic polar stratosphere, *Geophys. Res. Lett.*, *29*(8), 1184, doi:10.1029/2001GL014147, 2002.

Pawson, S., K. Labitzke, R. Lenschow, B. Naujokat, B. Rajewski, M. Wiesner, and R.-C. Wohlfahrt, *Climatology of the Northern Hemisphere Stratosphere Derived From Berlin Analyses. Part 1: Monthly Means*, *Meteorol. Abh., Ser. A: Monogr.*, vol. 7.3, 299 pp., D. Reimer, Berlin, 1993.

Pawson, S., et al., The GCM-reality intercomparison project for SPARC (GRIPS): Scientific issues and initial results, *Bull. Am. Meteorol. Soc.*, *81*, 781–796, 2000.

Ramaswamy, V., et al., Stratospheric temperature trends: observations and model simulations, *Rev. Geophys.*, *39*, 71–122, 2001.

Randel, W. J., and F. Wu, Cooling of the Arctic and Antarctic polar stratospheres due to ozone depletion, *J. Clim.*, *12*, 1467–1479, 1999.

Rasch, P. J., and M. Lawrence, Recent development in transport methods at NCAR, *MPI-Rep. 265*, pp. 65–75, Max-Planck-Inst. für Meteorol., Hamburg, Germany, 1998.

Rasch, P. J., and D. L. Williamson, On shape-preserving interpolation and semi-Lagrangian transport, *SIAM J. Sci. Stat. Comput.*, *11*, 656–687, 1990.

Rasch, P. J., B. A. Boville, and G. P. Brasseur, A three-dimensional general circulation model with coupled chemistry for the middle atmosphere, *J. Geophys. Res.*, *100*, 9041–9071, 1995.

Rayner, N. A., E. B. Horton, D. E. Parker, C. K. Folland, and R. B. Hackett, Version 2.2 of the global sea-ice and sea surface temperature data set, 1903–1994, *Clim. Res. Tech. Note 74*, Hadley Cent., Bracknell, England, 1996.

Riese, M., P. Spang, P. Preusse, M. Ern, M. Jarisch, D. Offermann, and K. H. Grossmann, Cryogenic Infrared Spectrometer and Telescopes for the Atmosphere (CRISTA) data processing and atmospheric temperature and trace gas retrieval, *J. Geophys. Res.*, *104*, 16,349–16,367, 1999.

Rind, D., J. Lerner, K. Shah, and R. Suozzo, Use of on-line tracers as a diagnostic tool in general circulation model development: 2. Transport between the troposphere and the stratosphere, *J. Geophys. Res.*, *104*, 9151–9167, 1999.

Roche, A. E., J. B. Kumer, J. L. Mergenthaler, G. A. Ely, W. G. Uplinger, T. C. James, and L. W. Steritt, The Cryogenic Limb Array Etalon Spectrometer (CLAES) on UARS: Experiment description and performance, *J. Geophys. Res.*, *98*, 10,777–10,798, 1993.

Roche, A. E., J. B. Kumer, J. L. Mergenthaler, R. W. Nightingale, W. G. Uplinger, G. A. Ely, J. F. Potter, D. J. Wuebbles, P. S. Connell, and D. E. Kinnison, Observations of lower-stratospheric $ClONO_2$, HNO_3, and aerosol by the UARS/CLAES experiment between January 1992 and April 1993, *J. Atmos. Sci.*, *51*, 2877–2902, 1994.

Roeckner, E., K. Arpe, L. Bengtsson, M. Christoph, M. Claussen, L. Dümenil, M. Esch, M. A. Giorgetta, U. Schlese, and U. Schulzweida, The atmospheric general circulation model ECHAM4: Model description and simulation of present-day climate, *MPI-Rep. 218*, Max-Planck-Inst. für Meteorol., Hamburg, Germany, 1996.

Roeckner, E., L. Bengtsson, J. Feichter, J. Lelieveld, and H. Rodhe, Transient climate change simulations with a coupled atmosphere-ocean GCM including the tropospheric sulfur cycle, *J. Clim.*, *12*, 3004–3032, 1999.

Roelofs, G.-J., J. Lelieveld, and R. van Dorland, A three-dimensional chemistry/general circulation model simulation of anthropogenically derived ozone in the troposphere and its radiative climate forcing, *J. Geophys. Res.*, *102*, 23,389–23,401, 1997.

Rosenlof, K. H., A. F. Tuck, K. K. Kelly, J. M. Russell III, and M. P. McCormick, Hemispheric asymmetries in water vapor and inferences about transport in the lower stratosphere, *J. Geophys. Res.*, *102*, 13,213–13,234, 1997.

Röth, E.-P., A fast algorithm to calculate the photonflux in optically dense media for use in photochemical models, *Ber. Bunsenges. Phys. Chem.*, *96*, 417–420, 1992.

Rotman, D. A., et al., Global Modeling Initiative assessment model: Model description, integration, and testing of the transport shell, *J. Geophys. Res.*, *106*, 1669–1691, 2001.

Russell, J. M., L. L. Gordley, J. H. Park, S. R. Drayson, A. Tuck, J. E. Harries, R. J. Cicerone, P. J. Crutzen, and J. E. Frederick, The Halogen Occultation Experiment, *J. Geophys. Res.*, *98*, 10,777–10,797, 1993.

Santee, M. L., L. Froidevaux, G. L. Manney, W. G. Read, J. W. Waters, M. P. Chipperfield, A. E. Roche, J. B. Kumer, J. L. Mergenthaler, and J. M. Russell III, Chlorine deactivation in the lower stratospheric polar regions during late winter: Results from UARS, *J. Geophys. Res.*, *101*, 18,835–18,859, 1996a.

Santee, M. L., G. L. Manney, W. G. Read, L. Froidevaux, and J. W. Waters, Polar vortex conditions during the 1995–96 Arctic winter, MLS ClO and HNO_3, *Geophys. Res. Lett.*, *23*, 3207–3210, 1996b.

Santee, M. L., G. L. Manney, L. Froidevaux, W. G. Read, and J. W. Waters, Six years of UARS Microwave Limb Sounder HNO_3 observations: Seasonal, interhemispheric, and interannual variations in the lower stratosphere, *J. Geophys. Res.*, *104*, 8225–8246, 1999.

Santee, M. L., G. L. Manney, N. J. Livesey, and J. W. Waters, UARS Microwave Limb Sounder observations of denitrification and ozone loss in the 2000 Arctic late winter, *Geophys. Res. Lett.*, *27*, 3213–3216, 2000.

Segers, A., P. van Velthoven, B. Bregman, and M. Krol, On the computation of mass fluxes for Eulerian transport models from spectral meteorological fields, *Lect. Notes Comput. Sci.*, *2330*, 767–776, 2002.

Shindell, D., D. Rind, and P. Lonergan, Increased polar stratospheric ozone losses and delayed eventual recovery owing to increasing greenhouse-gas concentrations, *Nature*, *392*, 589–592, 1998a.

Shindell, D., D. Rind, and P. Lonergan, Climate change and the middle atmosphere. part IV: Ozone response to doubled CO_2, *J. Clim.*, *11*, 895–918, 1998b.

Shine, K. P., On the modelled thermal response of the Antarctic stratosphere to a depletion of ozone, *Geophys. Res. Lett.*, *13*, 1331–1334, 1986.

Solomon, S., Stratospheric ozone depletion: A review of concepts and history, *Rev. Geophys.*, *37*, 275–316, 1999.

Sparling, L. C., Statistical perspectives on stratospheric transport, *Rev. Geophys.*, *38*, 417–436, 2000.

Steil, B., Modellierung der Chemie der Strato- und Troposphäre mit einem dreidimensionalen Zirkulationsmodell, dissertation, Inst. für Meteorol., Univ. Hamburg, Hamburg, Germany, 1999.

Steil, B., M. Dameris, C. Brühl, P. J. Crutzen, V. Grewe, M. Ponater, and R. Sausen, Development of a chemistry module for GCMs: First results of a multi-annual integration, *Ann. Geophys.*, *16*, 205–228, 1998.

Summers, M. E., R. R. Conway, D. E. Siskind, M. H. Stevens, D. Offermann, M. Riese, P. Preusse, D. F. Strobel, and P. M. Russell III, Implications of satellite OH observations for middle atmospheric H_2O and ozone, *Science*, *277*, 1967–1970, 1997.

von Kuhlmann, R., M. G. Lawrence, P. J. Crutzen, and P. J. Rasch, A model for studies of tropospheric ozone and nonmethane hydrocarbons: Model description and ozone results, *J. Geophys. Res.*, *108*, doi:10.1029/2002JD002893, in press, 2003.

Waibel, A., T. Peter, K. Carslaw, H. Oelhaf, G. Wetzel, P. J. Crutzen, U. Pöschl, A. Tsias, E. Reimer, and H. Fischer, Persistent ozone loss due to greenhouse-enhanced denitrification, *Science*, *283*, 2064–2069, 1999.

Waugh, D. W., W. J. Randel, S. Pawson, P. A. Newman, and E. R. Nash, Persistence of the lower stratospheric polar vortices, *J. Geophys. Res.*, *104*, 27,191–27,201, 1999.

World Meteorological Organization (WMO), Scientific assessment of ozone depletion: 1991, *Rep. 25*, Geneva, 1992.

World Meteorological Organization (WMO), Scientific assessment of ozone depletion: 1998, *Rep. 44*, Geneva, 1999.

C. Brühl, P. Crutzen, J. Lelieveld, and B. Steil, Air Chemistry Division, Max Planck Institute for Chemistry, P. O. Box 3060, 55020 Mainz, Germany. (steil@mpch-mainz.mpg.de)

K. Krüger, Institute for Meteorology, Free University of Berlin, Carl-Heinrich-Beckerweg 6–10, 12165 Berlin, Germany. (krueger@strat01.met.fu-berlin.de)

E. Manzini, National Institute for Geophysics and Volcanology, Via Gobetti 101, 40129 Bologna, Italy.

P. Rasch, National Center for Atmospheric Research, P. O. Box 3000, Boulder, CO 80307, USA. (pjr@ucar.edu)

E. Roeckner, Max-Planck-Institute for Meteorology, Bundesstraße 55, 20146 Hamburg, Germany. (roeckner@dkrz.de)